

# The $B(B_s) \rightarrow D_{(s)}(\bar{D}_{(s)})T$ and $D_{(s)}^*(\bar{D}_{(s)}^*)T$ decays in perturbative QCD approach

Zhi-Tian Zou, Xin Yu, and Cai-Dian Lü\*

*Institute of High Energy Physics and Theoretical Physics Center for Science Facilities,  
Chinese Academy of Sciences, Beijing 100049, People's Republic of China*

(Dated: April 15, 2019)

## Abstract

In perturbative QCD approach, we investigate the  $B(B_s) \rightarrow D_{(s)}(\bar{D}_{(s)})T$  and  $D_{(s)}^*(\bar{D}_{(s)}^*)T$  decays, which include the Cabibbo-Kobayashi-Maskawa (CKM) favored decays and the Cabibbo-Kobayashi-Maskawa-suppressed decays, where T denotes a light tensor meson. From our calculation, we find that the nonfactorizable emission diagrams and the annihilation type diagrams are important, especially for those color suppressed channels. For those decays with a tensor meson emitted, the factorizable emission diagrams vanish owing to the fact that a tensor meson can not be produced through the local (V-A) or tensor current. The numerical results show that the predictions for the branching ratios of considered charmed B decays are in the range of  $10^{-4}$  to  $10^{-6}$  for those CKM-favored decays (governed by  $|V_{cb}|$ ) and in the range of  $10^{-5}$  to  $10^{-8}$  for those CKM-suppressed decays (governed by  $|V_{ub}|$ ). We also predict large transverse polarization contributions in many of the  $B(B_s) \rightarrow D_{(s)}^*(\bar{D}_{(s)}^*)T$  decay channels.

PACS numbers: 13.25.Hw, 12.38.Bx

---

\*Electronic address: lucd@ihep.ac.cn

## I. INTRODUCTION

In the recent years, several experimental measurements about B decay modes involving a light tensor meson (T) have been obtained [1]. These light tensor mesons include the isovector  $a_2(1320)$ , the isodoublet  $K_2^*(1430)$ , and isosinglet  $f_2(1270)$  and  $f_2'(1525)$  [1]. For the tensor meson with  $J^P = 2^+$ , both the orbital angular momentum L and the total spin S of the quark pair are equal to 1. However, their production property in B decays is quite similar to the light vector mesons [2]. These rare B decays have been studied in the naive factorization [3–7]. Due to the fact that  $\langle 0 | j^\mu | T \rangle = 0$ , where  $j^\mu$  is the  $(V \pm A)$  or  $(S \pm P)$  current [3, 4, 8, 9], the factorizable amplitude with a tensor meson emitted vanishes. Therefore, the naive factorization approach for this kind of decays can not give the right prediction. The recent developed QCD factorization approach [8, 9] and the perturbative QCD factorization approach (PQCD) [10] overcome these shortcoming by including the large non-factorization contributions and the annihilation type contributions.

There is another category of B decays with a heavy  $D$  meson and a tensor meson in the final states, which are discussed in the factorization approach [11–16]. These  $B$  decays include the Cabibbo-Kobayashi-Maskawa- (CKM-)favored  $B$  decays through  $b \rightarrow c$  transition, and the CKM-suppressed  $B$  decays through  $b \rightarrow u$  transition. There are only tree operator contributions, thus no CP asymmetry appears in the standard model for these decays. Again, the factorizable diagrams with a tensor meson emitted vanish in the naive factorization. To deal with the large non-factorizable contribution and annihilation type contribution, one has to go beyond the naive factorization.

Recently, three pure annihilation type decays  $B^0 \rightarrow D_s^- K_2^{*+}$  and  $B_s \rightarrow \bar{D} a_2$  are calculated in the perturbative QCD approach, which give sizable branching ratios [17]. In this work, we shall extend the study to all the charmed  $B(B_s) \rightarrow D_{(s)}^{(*)}(\bar{D}_{(s)}^{(*)})T$  decays in the PQCD approach, which is based on the  $k_T$  factorization [18, 19]. We know that the light quark in B meson is soft, while it is collinear in the final state light meson, so a hard gluon is necessary to connect the spectator quark to the four quark operator. So the hard part of the PQCD approach contains six quarks rather than four quarks. This is called six-quark effective theory or six-quark operator. In the calculation of the factorizable diagrams and the annihilation type diagrams, endpoint singularity will appear

to spoil the perturbative calculation. In the conventional collinear factorization, people usually parameterize these singularity, thus makes the theoretical prediction weak. In the PQCD approach, the quarks' intrinsic transverse momenta are kept to avoid the endpoint divergence. Because of the additional energy scale introduced by the transverse momentum, double logarithms will appear in the QCD radiative corrections. We resum these double logarithms to give a Sudakov factor, which effectively suppresses the end-point region contribution. This makes the PQCD approach more reliable and consistent. So in the perturbative QCD approach, one can not only give predictions for the decays with a tensor meson emitted but also calculate the pure annihilation type B decays [20, 21].

In charmed B decays, there is one more intermediate energy scale, the heavy D meson mass. As a result, another expansion series of  $m_D/m_B$  will appear. The factorization is only approved at the leading of  $m_D/m_B$  expansion [22, 23]. It is also proved factorization in the soft collinear effective theory for this kind of decays [24]. Therefore, we will take only the leading order contribution into account, unless explicitly mentioned.

This paper is organized as following. In Section II, we present the formalism and wave functions of the considered B meson decays. Then we perform the perturbative calculations for considered decay channels with the PQCD approach in Sec.III. The numerical results and phenomenological analysis are given in Sec.IV. Finally, Sec.V is a short summary.

## II. FORMALISM AND WAVE FUNCTION

The  $B \rightarrow DT$  decays are weak decays through charged currents. At the quark level, there are only tree operator contributions, and the related weak effective Hamiltonian  $H_{eff}$  [25] can be written as

$$H_{eff} = \frac{G_F}{\sqrt{2}} V_{ub}^* V_{cd(s)} [C_1(\mu) O_1(\mu) + C_2(\mu) O_2(\mu)], \quad (1)$$

where  $V_{ub}$  and  $V_{cd(s)}$  are CKM matrix elements.  $C_{1,2}(\mu)$  are the Wilson coefficients at the renormalization scale  $\mu$ .  $O_{1,2}(\mu)$  are the four quark operators.

$$O_1 = (\bar{b}_\alpha u_\beta)_{V-A} (\bar{c}_\beta d(s)_\alpha)_{V-A}, \quad O_2 = (\bar{b}_\alpha u_\alpha)_{V-A} (\bar{c}_\beta d(s)_\beta)_{V-A}, \quad (2)$$

where  $\alpha$  and  $\beta$  are the color indices,  $(\bar{b}_\alpha u_\beta)_{V-A} = \bar{b}_\alpha \gamma^\mu (1 - \gamma^5) u_\beta$ . Conventionally, we define the combined Wilson coefficients as

$$a_1 = C_2 + C_1/3, \quad a_2 = C_1 + C_2/3. \quad (3)$$

For the  $B \rightarrow \bar{D}T$  decays, the decay rates will be enhanced comparing with the corresponding  $B \rightarrow DT$  decays by CKM matrix elements  $|V_{cb}/V_{ub}|^2$ . At quark level, these decays are governed by the effective Hamiltonian

$$H_{eff} = \frac{G_F}{\sqrt{2}} V_{cb}^* V_{ud(s)} [C_1(\mu) O_1(\mu) + C_2(\mu) O_2(\mu)], \quad (4)$$

with

$$O_1 = (\bar{b}_\alpha c_\beta)_{V-A} (\bar{u}_\beta d(s)_\alpha)_{V-A}, \quad O_2 = (\bar{b}_\alpha c_\alpha)_{V-A} (\bar{u}_\beta d(s)_\beta)_{V-A}. \quad (5)$$

In hadronic  $B$  decay calculations, one has to deal with the hadronization of mesons. In this calculation, there are three different scales: W boson mass scale, b quark mass scale  $M_B$  and the factorization scale  $\sqrt{\bar{\Lambda} M_B}$ , where  $\bar{\Lambda} \equiv M_B - m_b$ . The electroweak physics higher than W boson mass can be calculated perturbatively. The physics between b quark mass scale and W boson mass scale can be included in the Wilson coefficients of the effective four-quark operators, which is obtained by using the renormalization group equation. The physics between  $M_B$  and the factorization scale is included in the calculation of the hard part in the PQCD approach. The physics below the factorization scale is nonperturbative and described by the hadronic wave functions of mesons, which is universal for all decay modes. Therefore, the decay amplitude can be explicitly factorized into the convolution of the the Wilson coefficients, the hard scattering kernel and the light-cone wave functions of mesons characterized by different scales, respectively,

$$\begin{aligned} \mathcal{A} \sim & \int dx_1 dx_2 dx_3 b_1 db_1 b_2 db_2 b_3 db_3 \\ & \times Tr [C(t) \Phi_B(x_1, b_1) \Phi_{M_2}(x_2, b_2) \Phi_{M_3}(x_3, b_3) H(x_i, b_i, t) S_t(x_i) e^{-S(t)}], \end{aligned} \quad (6)$$

where  $b_i$  is the conjugate variable of quark's transverse momentum  $k_{iT}$ ,  $x_i$  is the momentum fractions of valence quarks, and  $t$  is the largest energy scale in the hard part  $H(x_i, b_i, t)$ .  $C(t)$  are the Wilson coefficients with resummation of the large logarithms  $\ln(m_W/t)$  produced by the radiative corrections.  $S_t(x_i)$  is the jet function, which is obtained by the threshold resummation and smears the end-point singularities on  $x_i$  [26].

The last term,  $e^{-S(t)}$ , is the Sudakov form factor which suppresses the soft dynamics effectively and suppresses the long distance contributions in the large  $b$  region [27, 28]. Thus it makes the perturbative calculation of the hard part  $H$  applicable at intermediate scale, i.e.,  $m_B$  scale.

In the PQCD approach, in order to calculate the decay amplitude, we should choose the proper wave functions for the initial and final state mesons. The initial B meson is a heavy pseudoscalar meson with two Lorentz structures in its wave function. We have neglected the numerically-suppressed one in the PQCD approach [29]. The two rest structure  $(\gamma_\mu \gamma_5)$  and  $\gamma_5$  components remain as leading contributions [2]. Then,  $\Phi_B$  can be written as

$$\Phi_B = \frac{i}{\sqrt{6}} [(\not{P} + m_B) \gamma_5 \phi_B(x)]. \quad (7)$$

For the distribution amplitude, we choose [29, 30]

$$\phi_B(x, b) = N_B x^2 (1-x)^2 \exp \left[ -\frac{1}{2} \left( \frac{m_B x}{\omega_B} \right)^2 - \frac{\omega_B^2 b^2}{2} \right], \quad (8)$$

where  $N_B$  is the normalization constant. We will take  $\omega_B = (0.4 \pm 0.04)$  GeV and  $f_B = (0.21 \pm 0.02)$  GeV for B meson [8, 9, 18, 29–31]. For the  $B_s$  meson, because of the SU(3) breaking effects, we choose  $\omega_{B_s} = (0.5 \pm 0.05)$  GeV [32] and  $f_{B_s} = (0.24 \pm 0.03)$  GeV.

For a tensor meson, the polarization tensor  $\epsilon_{\mu\nu}(\lambda)$  with helicity  $\lambda$  can be expanded through the polarization vectors  $\epsilon^\mu(0)$  and  $\epsilon^\mu(\pm 1)$  [8, 9]

$$\begin{aligned} \epsilon^{\mu\nu}(\pm 2) &\equiv \epsilon(\pm 1)^\mu \epsilon(\pm 1)^\nu, \\ \epsilon^{\mu\nu}(\pm 1) &\equiv \sqrt{\frac{1}{2}} [\epsilon(\pm 1)^\mu \epsilon(0)^\nu + \epsilon(0)^\mu \epsilon(\pm 1)^\nu], \\ \epsilon^{\mu\nu}(0) &\equiv \sqrt{\frac{1}{6}} [\epsilon(+1)^\mu \epsilon(-1)^\nu + \epsilon(-1)^\mu \epsilon(+1)^\nu] + \sqrt{\frac{2}{3}} \epsilon(0)^\mu \epsilon(0)^\nu. \end{aligned} \quad (9)$$

In order to calculate conveniently, we define a new polarization vector  $\epsilon_T$  for the considered tensor meson [2]

$$\epsilon_{T\mu} = \frac{1}{m_B} \epsilon_{\mu\nu}(h) P_B^\nu. \quad (10)$$

The new polarization vector  $\epsilon_T(\lambda)$  with helicity  $\lambda$  can be expressed as

$$\begin{aligned}\epsilon_{T\mu}(\pm 2) &= 0, \\ \epsilon_{T\mu}(\pm 1) &= \frac{1}{m_B} \frac{1}{\sqrt{2}} (\epsilon(0) \cdot P_B) \epsilon_\mu(\pm 1), \\ \epsilon_{T\mu}(0) &= \frac{1}{m_B} \sqrt{\frac{2}{3}} (\epsilon(0) \cdot P_B) \epsilon_\mu(0).\end{aligned}\tag{11}$$

In this convention, the  $\pm 2$  polarizations do not contribute, which is consistent with the angular momentum conservation argument in B decays. The  $\epsilon_T$  is similar with the  $\epsilon$  of vector state, regardless of the related constants [2]. This convention makes the following perturbative calculations simpler. After this simplification, the wave function for a generic tensor meson are defined by [2]

$$\begin{aligned}\Phi_T^L &= \frac{1}{\sqrt{6}} \left[ m_T \not{\epsilon}_{\bullet L}^* \phi_T(x) + \not{\epsilon}_{\bullet L}^* \not{P} \phi_T^t(x) + m_T^2 \frac{\epsilon_{\bullet} \cdot v}{P \cdot v} \phi_T^s(x) \right] \\ \Phi_T^\perp &= \frac{1}{\sqrt{6}} \left[ m_T \not{\epsilon}_{\bullet \perp}^* \phi_T^v(x) + \not{\epsilon}_{\bullet \perp}^* \not{P} \phi_T^T(x) + m_T i \epsilon_{\mu\nu\rho\sigma} \gamma_5 \gamma^\mu \epsilon_{\bullet \perp}^{*\nu} n^\rho v^\sigma \phi_T^a(x) \right].\end{aligned}\tag{12}$$

Here  $n$  is the moving direction of the tensor meson, and  $v$  is the opposite direction. We adopt the convention  $\epsilon^{0123} = 1$ . The vector  $\epsilon_{\bullet\mu} \equiv \frac{\epsilon_{\mu\nu} v^\nu}{P \cdot v}$  is related to the polarization tensor. The twist-2 and twist-3 distribution amplitudes are given by [2, 8, 9]

$$\begin{aligned}\phi_T(x) &= \frac{f_T}{2\sqrt{2N_c}} \phi_\parallel(x), \quad \phi_T^t = \frac{f_T^\perp}{2\sqrt{2N_c}} h_\parallel^{(t)}(x), \\ \phi_T^s(x) &= \frac{f_T^\perp}{4\sqrt{2N_c}} \frac{d}{dx} h_\parallel^{(s)}(x), \quad \phi_T^T(x) = \frac{f_T^\perp}{2\sqrt{2N_c}} \phi_\perp(x), \\ \phi_T^v(x) &= \frac{f_T}{2\sqrt{2N_c}} g_\perp^{(v)}(x), \quad \phi_T^a(x) = \frac{f_T}{8\sqrt{2N_c}} \frac{d}{dx} g_\perp^{(a)}(x),\end{aligned}\tag{13}$$

with the form

$$\begin{aligned}\phi_{\parallel,\perp}(x) &= 30x(1-x)(2x-1), \\ h_\parallel^{(t)}(x) &= \frac{15}{2}(2x-1)(1-6x+6x^2), \quad h_\parallel^{(s)}(x) = 15x(1-x)(2x-1), \\ g_\perp^{(a)}(x) &= 20x(1-x)(2x-1), \quad g_\perp^{(v)}(x) = 5(2x-1)^3.\end{aligned}\tag{14}$$

It is obvious that all the above light-cone distribution amplitudes (LCDAs) of the tensor meson are antisymmetric under the interchange of momentum fractions of the quark and anti-quark in the SU(3) limit (i.e.  $x \leftrightarrow 1-x$ ) [8, 9]. This is required by the Bose statistics, and consistent with the fact that  $\langle 0 | j^\mu | T \rangle = 0$ , where  $j^\mu$  is the  $(V \pm A)$  or  $(S \pm P)$  current.

For  $D^{(*)}$  meson, in the heavy quark limit, the two-parton LCDAs can be written as [33–36]

$$\begin{aligned}\langle D(p) | q_\alpha(z) \bar{c}_\beta(0) | 0 \rangle &= \frac{i}{\sqrt{2N_c}} \int_0^1 dx e^{ixp \cdot z} [\gamma_5 (\not{P} + m_D) \phi_D(x, b)]_{\alpha\beta}, \\ \langle D^*(p) | q_\alpha(z) \bar{c}_\beta(0) | 0 \rangle &= -\frac{1}{\sqrt{2N_c}} \int_0^1 dx e^{ixp \cdot z} [\not{\epsilon}_L (\not{P} + m_{D^*}) \phi_{D^*}^L(x, b) \\ &\quad + \not{\epsilon}_T (\not{P} + m_{D^*}) \phi_{D^*}^T(x, b)]_{\alpha\beta}.\end{aligned}\quad (15)$$

For the distribution amplitude for  $D^{(*)}$  meson, we take the same as that used in Refs. [34–36].

$$\phi_D(x, b) = \phi_{D^*}^{L(T)}(x, b) = \frac{1}{2\sqrt{2N_c}} f_{D^{(*)}} 6x(1-x) [1 + C_D(1-2x)] \exp\left[\frac{-\omega^2 b^2}{2}\right], \quad (16)$$

with  $C_D = 0.5 \pm 0.1$ ,  $\omega = 0.1$  GeV and  $f_D = 207$  MeV [37] for  $D(\bar{D})$  meson and  $C_D = 0.4 \pm 0.1$ ,  $\omega = 0.2$  GeV and  $f_{D_s} = 241$  MeV [37] for  $D_s(\bar{D}_s)$  meson. For  $D_{(s)}^*$  meson, we determine the decay constant of  $D_{(s)}^*$  meson by using the following relation based on heavy quark effective theory (HQET) [38]

$$f_{D_{(s)}^*} = \sqrt{\frac{m_{D_{(s)}}}{m_{D_{(s)}}^*}} f_{D_{(s)}}. \quad (17)$$

### III. PERTURBATIVE CALCULATION

In this section, we shall calculate the hard part  $H(t)$ , which is decay channel dependent. It includes the four quark operators and the necessary hard gluon connecting the four quark operator and the spectator quark [28]. We will express the whole amplitude for each diagram as the convolution of the hard kernel and wave functions.

There are 8 types of diagrams contributing to the  $B \rightarrow DT$  decays ( $\bar{b} \rightarrow c$  transition), which are shown in Fig.1. They are governed by the CKM matrix element  $V_{ub}$ , which are usually called CKM suppressed decay channels. The first two diagrams of Fig.1 are the factorizable diagrams. Their decay amplitude can be factorized as a product of the decay constant of  $D^{(*)}$  meson and a B to tensor meson transition form factor in the naive factorization approach. In the PQCD approach, we calculate these two diagrams and

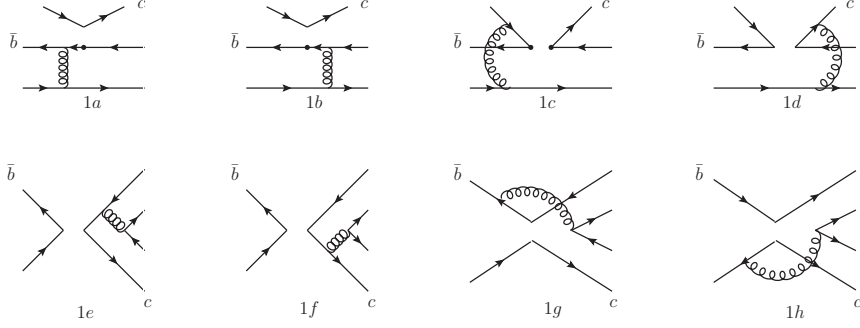


FIG. 1: Leading order Feynman diagrams contributing to the  $B \rightarrow D^{(*)}T$  decays in PQCD

obtain the decay amplitude as

$$\begin{aligned}
\mathcal{A}_{ef} = & -8\sqrt{\frac{2}{3}}\pi C_F m_B^4 f_D \int_0^1 dx_1 dx_3 \int_0^{1/\Lambda} b_1 db_1 b_3 db_3 \phi_B(x_1, b_1) \\
& \times \left\{ [\phi_T(x_3)(x_3 + 1) - (\phi_T^s(x_3) + \phi_T^t(x_3))r_T(2x_3 - 1)] \right. \\
& \cdot E_{ef}(t_a) h_{ef}(x_1, x_3(1 - r_D^2), b_1, b_3) \\
& \left. + 2r_T \phi_T^s(x_3) E_{ef}(t_b) h_{ef}(x_3, x_1(1 - r_D^2), b_3, b_1) \right\}, \tag{18}
\end{aligned}$$

with  $r_T = \frac{m_T}{m_B}$  and  $r_D = \frac{m_D}{m_B}$ .  $\phi_T^{(s,t)}(x_i)$  is the distribution amplitude of the tensor meson and  $C_F = \frac{4}{3}$  is a color factor. The functions  $h_{ef}$ ,  $t_{a,b}$ ,  $S_t$  and  $E_{ef}$  can be found in Appendix A.

For diagrams Fig.(1c) and (1d), which are the non-factorizable in naive factorization, the decay amplitudes involve all three meson wave functions. The integration of  $b_3$  can be performed through  $\delta$  function  $\delta(b_1 - b_3)$ , leaving only integration of  $b_1$  and  $b_2$ .

$$\begin{aligned}
\mathcal{M}_{enf} = & -\frac{32}{3}C_F\pi m_B^4 \int_0^1 dx_1 dx_2 dx_3 \int_0^{1/\Lambda} b_1 db_1 b_2 db_2 \phi_B(x_1, b_1) \phi_D(x_2, b_2) \\
& \times \left\{ [\phi_T(x_3)x_2 + (\phi_T^t(x_3) - \phi_T^s(x_3))r_T x_3] \right. \\
& \cdot h_{enf1}(x_i, b_i) E_{enf}(t_c) \\
& + [\phi_T(x_3)(x_2 - x_3 - 1) + (\phi_T^s(x_3) + \phi_T^t(x_3))r_T x_3] \\
& \left. \cdot h_{enf2}(x_i, b_i) E_{enf}(t_d) \right\}. \tag{19}
\end{aligned}$$

For the factorizable annihilation type diagrams Fig.(1e) and (1f), the decay amplitudes



involve only the final state meson wave functions, with the B meson factorized out,

$$\begin{aligned}
\mathcal{A}_{af} = & 8\sqrt{\frac{2}{3}}C_F f_B \pi m_B^4 \int_0^1 dx_2 dx_3 \int_0^{1/\Lambda} b_2 db_2 b_3 db_3 \phi_D(x_3, b_3) \\
& \times \{ [\phi_T(x_2)x_3 + 2r_D r_T \phi_T^s(x_2)(x_3 + 1)] \\
& \cdot h_{af}(x_2, x_3(1 - r_D^2), b_2, b_3) E_{af}(t_e) \\
& - [\phi_T(x_2)x_2 + r_D r_T (\phi_T^t(x_2)(2x_2 - 1) + \phi_T^s(x_2)(2x_2 + 1))] \\
& \cdot h_{af}(x_3, x_2(1 - r_D^2), b_3, b_2) E_{af}(t_f) \}. \tag{20}
\end{aligned}$$

For the non-factorizable annihilation diagrams Fig.(1g) and (1h), all three meson wave functions are involved in the decay amplitudes. The integration of  $b_3$  can be performed by the  $\delta$  function  $\delta(b_2 - b_3)$  to give the decay amplitudes as

$$\begin{aligned}
\mathcal{M}_{anf} = & \frac{32}{3}C_F \pi m_B^4 \int_0^1 dx_1 dx_2 dx_3 \int_0^{1/\Lambda} b_1 db_1 b_2 db_2 \phi_B(x_1, b_1) \phi_D(x_3, b_2) \\
& \times \{ [\phi_T(x_2)x_2 + r_D r_T (\phi_T^t(x_2)(x_2 - x_3) + \phi_T^s(x_2)(x_2 + x_3 + 2))] \\
& \cdot h_{anf1}(x_1, x_2, x_3, b_1, b_2) E_{anf}(t_g) \\
& - [\phi_T(x_2)x_3 + r_D r_T (\phi_T^t(x_2)(x_3 - x_2) + \phi_T^s(x_2)(x_2 + x_3))] \\
& \cdot h_{anf2}(x_1, x_2, x_3, b_1, b_2) E_{anf}(t_h) \}. \tag{21}
\end{aligned}$$

The situation for  $B \rightarrow D^*(\bar{D}^*)T$  mode is a little more complicated. Both the longitudinal polarization and the transverse polarization contribute. Their decay amplitude can be given by

$$\mathcal{A}(\epsilon_D, \epsilon_T) = i\mathcal{A}^L + i(\epsilon_D^{T*} \cdot \epsilon_T^{T*})\mathcal{A}^T + (\epsilon_{\mu\nu\alpha\beta} n^\mu v^\nu \epsilon_D^{T*\alpha} \epsilon_T^{T*\beta})\mathcal{A}^N, \tag{22}$$

where  $\mathcal{A}^L$  is the longitudinally polarized decay amplitude and  $\mathcal{A}^T$  and  $\mathcal{A}^N$  are the transversely polarized contributions.  $\epsilon_D^T$  is the transverse polarization vector of  $D^*(\bar{D}^*)$  and  $\epsilon_T^T$  is the vector used to construct the polarization tensors of the tensor meson.

For  $B \rightarrow D^*T$  decay mode, the longitudinally polarized expressions of factorizable and nonfactorizable emission contributions can be obtained by making the following substitutions in Eq.(18) and Eq.(19),

$$\phi_D \rightarrow \phi_{D^*}^L, \quad f_D \rightarrow f_{D^*}, \quad m_D \rightarrow m_{D^*}. \tag{23}$$

For annihilation type diagrams, the longitudinal decay amplitudes are

$$\begin{aligned}
\mathcal{A}_{af}^L = & 8\sqrt{\frac{2}{3}}C_F f_B \pi m_B^4 \int_0^1 dx_2 dx_3 \int_0^{1/\Lambda} b_2 db_2 b_3 db_3 \phi_D^L(x_3, b_3) \\
& \times \{ [\phi_T(x_2)x_3 + 2r_D r_T \phi_T^s(x_2)(x_3 - 1)] \\
& \cdot h_{af}(x_2, x_3(1 - r_D^2), b_2, b_3) E_{af}(t_e) \\
& - [\phi_T(x_2)x_2 + r_D r_T (\phi_T^s(x_2) - \phi_T^t(x_2))] \\
& \cdot h_{af}(x_3, x_2(1 - r_D^2), b_3, b_2) E_{af}(t_f) \} , \tag{24}
\end{aligned}$$

$$\begin{aligned}
\mathcal{M}_{anf}^L = & \frac{32}{3}C_F \pi m_B^4 \int_0^1 dx_1 dx_2 dx_3 \int_0^{1/\Lambda} b_1 db_1 b_2 db_2 \phi_B(x_1, b_1) \phi_D^L(x_3, b_2) \\
& \times \{ [\phi_T(x_2)x_2 + r_D r_T (\phi_T^s(x_2)(x_2 - x_3) + \phi_T^t(x_2)(x_2 + x_3 - 2))] \\
& \cdot h_{anf1}(x_1, x_2, x_3, b_1, b_2) E_{anf}(t_g) \\
& + [-\phi_T(x_2)x_3 + r_D r_T (\phi_T^s(x_2)(x_2 - x_3) - \phi_T^t(x_2)(x_2 + x_3))] \\
& \cdot h_{anf2}(x_1, x_2, x_3, b_1, b_2) E_{anf}(t_h) \} . \tag{25}
\end{aligned}$$

The transversely polarized contributions are suppressed by  $r_D$  or  $r_T$ , whose decay amplitudes can be given by

$$\begin{aligned}
\mathcal{A}_{ef}^T = & -4\sqrt{2}\pi C_F m_B^4 f_{D^*} r_D \int_0^1 dx_1 dx_3 \int_0^{1/\Lambda} b_1 db_1 b_3 db_3 \phi_B(x_1, b_1) \\
& \times \{ [\phi_T^T(x_3) + r_T (\phi_T^v(x_3)(x_3 + 2) - \phi_T^a(x_3)x_3)] \\
& \cdot E_{ef}(t_a) h_{ef}(x_1, x_3(1 - r_D^2), b_1, b_3) \\
& + r_T (\phi_T^a(x_3) + \phi_T^v(x_3)) E_{ef}(t_b) h_{ef}(x_3, x_1(1 - r_D^2), b_3, b_1) \} , \tag{26}
\end{aligned}$$

$$\mathcal{A}_{ef}^N = \mathcal{A}_{ef}^T(\phi_T^a \leftrightarrow \phi_T^v), \tag{27}$$

$$\begin{aligned}
\mathcal{M}_{enf}^T = & 16\sqrt{\frac{1}{3}}C_F \pi m_B^4 r_D \int_0^1 dx_1 dx_2 dx_3 \int_0^{1/\Lambda} b_1 db_1 b_2 db_2 \phi_B(x_1, b_1) \phi_D^T(x_2, b_2) \\
& \times \{ [-\phi_T^T(x_3)x_2] h_{enf1}(x_i, b_i) E_{enf}(t_c) \\
& + [\phi_T^T(x_3)(x_2 + 1) + r_T (\phi_T^v(x_3)(1 - 2x_2 + 2x_3) - \phi_T^a(x_3))] \\
& \cdot h_{enf2}(x_i, b_i) E_{enf}(t_d) \} , \tag{28}
\end{aligned}$$

$$\mathcal{M}_{enf}^N = \mathcal{M}_{enf}^T(\phi_T^a \leftrightarrow \phi_T^v), \tag{29}$$

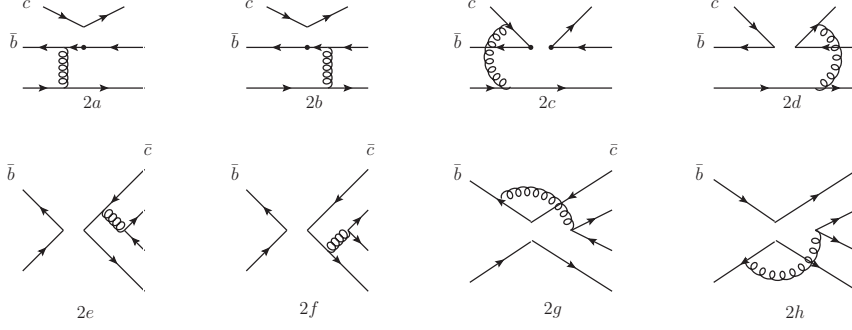


FIG. 2: Leading order Feynman diagrams contributing to the  $B \rightarrow \bar{D}T$  decays

$$\begin{aligned}
\mathcal{A}_{af}^T = & 4\sqrt{2}C_F f_B \pi m_B^4 r_D \int_0^1 dx_2 dx_3 \int_0^{1/\Lambda} b_2 db_2 b_3 db_3 \phi_D^T(x_3, b_3) \\
& \times \{r_T [\phi_T^a(x_2)(1-x_3) + \phi_T^v(x_2)(x_3+1)] \\
& \cdot h_{af}(x_2, x_3(1-r_D^2), b_2, b_3) E_{af}(t_e) \\
& + [r_D \phi_T^T(x_2) + r_T(\phi_T^a(x_2)(1-x_2) - \phi_T^v(x_2)(x_2+1))] \\
& \cdot h_{af}(x_3, x_2(1-r_D^2), b_3, b_2) E_{af}(t_f)\}, \tag{30}
\end{aligned}$$

$$\mathcal{A}_{af}^N = -\mathcal{A}_{af}^T(\phi_T^a \leftrightarrow \phi_T^v), \tag{31}$$

$$\begin{aligned}
\mathcal{M}_{anf}^T = & 16\sqrt{\frac{1}{3}} C_F \pi m_B^4 r_D \int_0^1 dx_1 dx_2 dx_3 \int_0^{1/\Lambda} b_1 db_1 b_2 db_2 \phi_B(x_1, b_1) \phi_D^T(x_3, b_2) \\
& \times \{[2r_T \phi_T^v(x_2) + r_D \phi_T^T(x_2)(x_3-1)] h_{anf1}(x_1, x_2, x_3, b_1, b_2) E_{anf}(t_g) \\
& - [r_D x_3 \phi_T^T(x_2)] h_{anf2}(x_1, x_2, x_3, b_1, b_2) E_{anf}(t_h)\}. \tag{32}
\end{aligned}$$

$$\mathcal{M}_{anf}^N = -\mathcal{M}_{anf}^T(\phi_T^v \rightarrow \phi_T^a). \tag{33}$$

The complete decay amplitudes of each  $B_{(s)} \rightarrow D_{(s)} T$  channels are then

$$\mathcal{A}(B^0 \rightarrow D^0 a_2^0) = \frac{G_F}{\sqrt{2}} \frac{1}{\sqrt{2}} V_{ub}^* V_{cd} [a_2 \mathcal{A}_{af} + C_2 \mathcal{M}_{anf} - a_2 \mathcal{A}_{ef} - C_2 \mathcal{M}_{enf}], \quad (34)$$

$$\mathcal{A}(B^0 \rightarrow D^0 f_2^q) = \frac{G_F}{\sqrt{2}} \frac{1}{\sqrt{2}} V_{ub}^* V_{cd} [a_2 \mathcal{A}_{ef} + C_2 \mathcal{M}_{enf} + a_2 \mathcal{A}_{af} + C_2 \mathcal{M}_{anf}], \quad (35)$$

$$\mathcal{A}(B^0 \rightarrow D^0 K_2^{*0}) = \frac{G_F}{\sqrt{2}} V_{ub}^* V_{cs} [a_2 \mathcal{A}_{ef} + C_2 \mathcal{M}_{enf}], \quad (36)$$

$$\mathcal{A}(B^0 \rightarrow D^+ a_2^-) = \frac{G_F}{\sqrt{2}} V_{ub}^* V_{cd} [a_1 \mathcal{A}_{ef} + C_1 \mathcal{M}_{enf} + a_2 \mathcal{A}_{af} + C_2 \mathcal{M}_{anf}], \quad (37)$$

$$\mathcal{A}(B^0 \rightarrow D_s^+ a_2^-) = \frac{G_F}{\sqrt{2}} V_{ub}^* V_{cs} [a_1 \mathcal{A}_{ef} + C_1 \mathcal{M}_{enf}], \quad (38)$$

$$\mathcal{A}(B^0 \rightarrow D_s^+ K_2^{*-}) = \frac{G_F}{\sqrt{2}} V_{ub}^* V_{cd} [a_2 \mathcal{A}_{af} + C_2 \mathcal{M}_{anf}], \quad (39)$$

$$\mathcal{A}(B^+ \rightarrow D^0 a_2^+) = \frac{G_F}{\sqrt{2}} V_{ub}^* V_{cd} [a_2 \mathcal{A}_{ef} + C_2 \mathcal{M}_{enf} + a_1 \mathcal{A}_{af} + C_1 \mathcal{M}_{anf}], \quad (40)$$

$$\mathcal{A}(B^+ \rightarrow D^0 K_2^{*+}) = \frac{G_F}{\sqrt{2}} V_{ub}^* V_{cs} [a_2 \mathcal{A}_{ef} + C_2 \mathcal{M}_{enf} + a_1 \mathcal{A}_{af} + C_1 \mathcal{M}_{anf}] \quad (41)$$

$$\mathcal{A}(B^+ \rightarrow D^+ a_2^0) = \frac{G_F}{\sqrt{2}} \frac{1}{\sqrt{2}} V_{ub}^* V_{cd} [a_1 \mathcal{A}_{ef} + C_1 \mathcal{M}_{enf} - a_1 \mathcal{A}_{af} - C_1 \mathcal{M}_{anf}], \quad (42)$$

$$\mathcal{A}(B^+ \rightarrow D^+ f_2^q) = \frac{G_F}{\sqrt{2}} \frac{1}{\sqrt{2}} V_{ub}^* V_{cd} [a_1 \mathcal{A}_{ef} + C_1 \mathcal{M}_{enf} + a_1 \mathcal{A}_{af} + C_1 \mathcal{M}_{anf}], \quad (43)$$

$$\mathcal{A}(B^+ \rightarrow D^+ K_2^{*0}) = \frac{G_F}{\sqrt{2}} V_{ub}^* V_{cs} [a_1 \mathcal{A}_{af} + C_1 \mathcal{M}_{anf}], \quad (44)$$

$$\mathcal{A}(B^+ \rightarrow D_s^+ a_2^0) = \frac{G_F}{\sqrt{2}} \frac{1}{\sqrt{2}} V_{ub}^* V_{cs} [a_1 \mathcal{A}_{ef} + C_1 \mathcal{M}_{enf}], \quad (45)$$

$$\mathcal{A}(B^+ \rightarrow D_s^+ f_2^q) = \frac{G_F}{\sqrt{2}} \frac{1}{\sqrt{2}} V_{ub}^* V_{cs} [a_1 \mathcal{A}_{ef} + C_1 \mathcal{M}_{enf}], \quad (46)$$

$$\mathcal{A}(B^+ \rightarrow D_s^+ f_2^s) = \frac{G_F}{\sqrt{2}} V_{ub}^* V_{cs} [a_1 \mathcal{A}_{af} + C_1 \mathcal{M}_{anf}], \quad (47)$$

$$\mathcal{A}(B^+ \rightarrow D_s^+ \bar{K}_2^{*0}) = \frac{G_F}{\sqrt{2}} V_{ub}^* V_{cd} [a_1 \mathcal{A}_{af} + C_1 \mathcal{M}_{anf}], \quad (48)$$

$$\mathcal{A}(B_s^0 \rightarrow D^0 a_2^0) = \frac{G_F}{\sqrt{2}} \frac{1}{\sqrt{2}} V_{ub}^* V_{cs} [a_2 \mathcal{A}_{af} + C_2 \mathcal{M}_{anf}], \quad (49)$$

$$\mathcal{A}(B_s^0 \rightarrow D^0 f_2^q) = \frac{G_F}{\sqrt{2}} \frac{1}{\sqrt{2}} V_{ub}^* V_{cs} [a_2 \mathcal{A}_{af} + C_2 \mathcal{M}_{anf}], \quad (50)$$

$$\mathcal{A}(B_s^0 \rightarrow D^0 f_2^s) = \frac{G_F}{\sqrt{2}} V_{ub}^* V_{cs} [a_2 \mathcal{A}_{ef} + C_2 \mathcal{M}_{enf}], \quad (51)$$

$$\mathcal{A}(B_s^0 \rightarrow D^0 \bar{K}_2^{*0}) = \frac{G_F}{\sqrt{2}} V_{ub}^* V_{cd} [a_2 \mathcal{A}_{ef} + C_2 \mathcal{M}_{enf}], \quad (52)$$

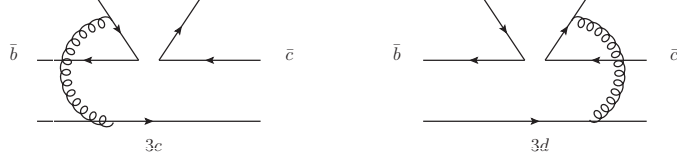


FIG. 3: Feynman diagrams contributing to the  $B \rightarrow \bar{D}T$  decays with a tensor meson emitted

$$\mathcal{A}(B_s^0 \rightarrow D^+ a_2^-) = \frac{G_F}{\sqrt{2}} V_{ub}^* V_{cs} [a_2 \mathcal{A}_{af} + C_2 \mathcal{M}_{anf}], \quad (53)$$

$$\mathcal{A}(B_s^0 \rightarrow D^+ K_2^{*-}) = \frac{G_F}{\sqrt{2}} V_{ub}^* V_{cd} [a_1 \mathcal{A}_{ef} + C_1 \mathcal{M}_{enf}], \quad (54)$$

$$\mathcal{A}(B_s^0 \rightarrow D_s^+ K_2^{*-}) = \frac{G_F}{\sqrt{2}} V_{ub}^* V_{cs} [a_1 \mathcal{A}_{ef} C_1 \mathcal{M}_{enf} + a_2 \mathcal{A}_{af} + C_2 \mathcal{M}_{anf}]. \quad (55)$$

From Eq.(A1), we know that

$$\mathcal{A}(B_{(s)} \rightarrow D^{(*)} f_2) = \mathcal{A}(B_{(s)} \rightarrow D^{(*)} f_2^q) \cos \theta + \mathcal{A}(B_{(s)} \rightarrow D^{(*)} f_2^s) \sin \theta, \quad (56)$$

$$\mathcal{A}(B_{(s)} \rightarrow D^{(*)} f_2') = \mathcal{A}(B_{(s)} \rightarrow D^{(*)} f_2^q) \sin \theta - \mathcal{A}(B_{(s)} \rightarrow D^{(*)} f_2^s) \cos \theta, \quad (57)$$

with  $\theta = 7.8^\circ$ .

The diagrams for  $\bar{b} \rightarrow \bar{c}$  decays are shown in Fig.2 and Fig.3. The CKM favored decays are governed by the larger CKM matrix element  $V_{cb}$ , then with a larger branching ratio. Because a tensor meson can not be produced through the  $(V \pm A)$  or tensor current, there are no factorizable emission diagrams with a tensor meson emitted in Fig.3. We collect the decay amplitudes for each  $\bar{b} \rightarrow \bar{c}$  decays in Appendix B.

#### IV. NUMERICAL RESULTS AND DISCUSSIONS

The decay width of a  $B$  meson at rest decaying into  $D(\bar{D})$  and  $T$  is

$$\Gamma(B \rightarrow D(\bar{D})T) = \frac{|\vec{P}|}{8\pi m_B^2} |\mathcal{A}(B \rightarrow D(\bar{D})T)|^2, \quad (58)$$

where the momentum of the final state particle is given by

$$|\vec{P}| = \frac{1}{2m_B} \sqrt{[m_B^2 - (m_D + m_T)^2][m_B^2 - (m_D - m_T)^2]}. \quad (59)$$

TABLE I: Branching ratios of  $B_{(s)} \rightarrow DT$  decays calculated in the PQCD approach together with results from Isgur-Scora-Grinstein-Wise (ISGW) II model [14, 15] (unit:  $10^{-7}$ ).

Decay Modes	Class	This Work	SDV[14]	KLO[15]
$B^0 \rightarrow D^0 a_2^0$	C	$0.55^{+0.28+0.15+0.10}_{-0.20-0.15-0.08}$	0.34	...
$B^0 \rightarrow D^0 f_2$	C	$2.05^{+0.81+0.34+0.27}_{-0.71-0.29-0.24}$	0.36	...
$B^0 \rightarrow D^0 f_2'$	C	$0.038^{+0.015+0.006+0.005}_{-0.013-0.006-0.005}$	0.0071	...
$B^0 \rightarrow D^0 K_2^{*0}$	C	$41.8^{+17.4+7.50+5.75}_{-14.1-7.04-5.36}$	12	11
$B^0 \rightarrow D^+ a_2^-$	T	$15.2^{+7.82+1.97+1.96}_{-6.31-2.62-1.80}$	12	...
$B^0 \rightarrow D_s^+ a_2^-$	T	$521^{+249+44+72}_{-189-60-65}$	380	180
$B^0 \rightarrow D_s^+ K_2^{*-}$	E	$0.61^{+0.15+0.12+0.08}_{-0.14-0.16-0.07}$	...	...
$B^+ \rightarrow D^0 a_2^+$	C	$1.95^{+0.81+0.41+0.24}_{-0.70-0.48-0.24}$	0.73	...
$B^+ \rightarrow D^0 K_2^{*+}$	C	$37.3^{+14.3+6.99+5.10}_{-12.4-8.32-4.67}$	13	12
$B^+ \rightarrow D^+ a_2^0$	T	$9.40^{+4.59+1.15+1.20}_{-3.39-1.62-1.12}$	6.5	...
$B^+ \rightarrow D^+ f_2$	T	$12.9^{+6.31+0.90+1.60}_{-5.31-1.42-1.50}$	6.9	...
$B^+ \rightarrow D^+ f_2'$	T	$0.24^{+0.12+0.02+0.03}_{-0.09-0.02-0.03}$	1.4	...
$B^+ \rightarrow D^+ K_2^{*0}$	A	$5.27^{+1.78+0.69+0.72}_{-1.65-0.66-0.66}$	...	...
$B^+ \rightarrow D_s^+ a_2^0$	T	$280^{+134+23+38}_{-110-33-35}$	200	94
$B^+ \rightarrow D_s^+ f_2$	T	$299^{+149+26+41}_{-122-33-37}$	220	100
$B^+ \rightarrow D_s^+ f_2'$	T,A	$4.12^{+1.69+1.62+0.57}_{-1.98-0.78-0.51}$	4.3	1.2
$B^+ \rightarrow D_s^+ \bar{K}_2^{*0}$	A	$0.34^{+0.12+0.06+0.04}_{-0.10-0.06-0.04}$	...	...
$B_s \rightarrow D^0 a_2^0$	E	$3.87^{+1.35+0.69+0.53}_{-1.19-0.95-0.48}$	...	...
$B_s \rightarrow D^0 f_2$	E	$6.26^{+2.29+1.00+0.53}_{-1.99-1.18-0.48}$	0.15	...
$B_s \rightarrow D^0 f_2'$	C	$25.5^{+12.5+4.00+3.5}_{-11.4-3.35-3.2}$	10	...
$B_s \rightarrow D^0 \bar{K}_2^{*0}$	C	$1.42^{+0.69+0.24+0.18}_{-0.55-0.19-0.17}$	0.46	...
$B_s \rightarrow D^+ a_2^-$	E	$8.06^{+3.03+1.43+1.11}_{-2.68-1.99-1.00}$	...	...
$B_s \rightarrow D^+ K_2^{*-}$	T	$11.2^{+5.61+0.60+1.46}_{-4.51-0.71-1.33}$	8.3	...
$B_s \rightarrow D_s^+ K_2^{*-}$	T	$206^{+115+16+28}_{-95-26-25}$	260	...

For  $B \rightarrow D^*(\bar{D}^*)T$  decays, the decay width can be written as

$$\Gamma(B \rightarrow D^*(\bar{D}^*)T) = \frac{|\vec{P}|}{8\pi m_B^2} \sum_{i=+,-,0} |\mathcal{A}_i(B \rightarrow D^*(\bar{D}^*)T)|^2, \quad (60)$$

where the three polarization amplitudes  $\mathcal{A}_i$  are given by

$$\mathcal{A}_0 = \mathcal{A}^L, \quad \mathcal{A}_{\pm} = \mathcal{A}^T \pm \mathcal{A}^N. \quad (61)$$

All the input parameters, such as decay constants, CKM elements are given in Appendix A, if not given in the previous two sections. The numerical results of branching

TABLE II: Branching ratios (unit: $10^{-7}$ ) and the percentage of transverse polarizations  $R_T$ (unit:%) of  $B_{(s)} \rightarrow D^*T$  decays calculated in the PQCD approach together with results from ISGW II model [14, 15].

Decay Modes	Class	Branching Ratio			$R_T$
		This Work	SDV[14]	KLO[15]	
$B^0 \rightarrow D^{*0}a_2^0$	C	$1.34^{+0.64+0.25+0.17}_{-0.53-0.19-0.15}$	0.50	...	$47^{+3.7+1.4}_{-4.5-1.6}$
$B^0 \rightarrow D^{*0}f_2$	C	$2.70^{+1.22+0.43+0.36}_{-1.02-0.30-0.33}$	0.53	...	$26^{+3.7+1.3}_{-4.0-1.1}$
$B^0 \rightarrow D^{*0}f_2'$	C	$0.052^{+0.023+0.008+0.007}_{-0.02-0.005-0.006}$	0.01	...	$26^{+3.7+1.3}_{-4.0-1.1}$
$B^0 \rightarrow D^{*0}K_2^{*0}$	C	$60.5^{+25.3+10.6+8.30}_{-21.3-9.15-7.56}$	19	18	$22^{+2.7+1.0}_{-3.2-0.5}$
$B^0 \rightarrow D^{*+}a_2^-$	T	$21.6^{+10.6+2.48+2.90}_{-8.60-3.10-2.50}$	18	...	$28^{+1.6+1.7}_{-1.5-1.6}$
$B^0 \rightarrow D_s^{*+}a_2^-$	T	$688^{+321+55+94}_{-267-79-86}$	367	291	$26^{+1.2+0.4}_{-0.9-0.7}$
$B^0 \rightarrow D_s^{*+}K_2^{*-}$	E	$0.57^{+0.13+0.12+0.07}_{-0.13-0.11-0.07}$	...	...	$12^{+1.6+3.2}_{-1.6-2.5}$
$B^+ \rightarrow D^{*0}a_2^+$	C	$4.46^{+2.01+0.73+0.58}_{-1.65-0.61-0.53}$	1.1	...	$41^{+3.8+2.3}_{-3.6-1.6}$
$B^+ \rightarrow D^{*0}K_2^{*+}$	C	$72.1^{+28.3+11.8+10.}_{-23.7-9.38-9.00}$	21	19	$35^{+4.0+0.9}_{-3.6-1.0}$
$B^+ \rightarrow D^{*+}a_2^0$	T	$14.0^{+6.51+1.03+1.80}_{-5.45-1.34-1.65}$	9.6	...	$25^{+1.5+0.3}_{-1.0-0.1}$
$B^+ \rightarrow D^{*+}f_2$	T	$15.1^{+8.83+1.42+2.01}_{-6.27-2.15-1.90}$	10	...	$25^{+1.3+1.8}_{-1.0-1.8}$
$B^+ \rightarrow D^{*+}f_2'$	T	$0.29^{+0.15+0.03+0.02}_{-0.11-0.04-0.02}$	0.21	...	$25^{+1.3+1.8}_{-1.0-1.8}$
$B^+ \rightarrow D^{*+}K_2^{*0}$	A	$18.2^{+4.77+0.21+2.00}_{-5.15-2.15-2.70}$	...	...	$82^{+2.1+3.8}_{-2.9-2.7}$
$B^+ \rightarrow D_s^{*+}a_2^0$	T	$330^{+155+27+45}_{-127-37-42}$	196	155	$26^{+1.2+0.4}_{-0.8-0.7}$
$B^+ \rightarrow D_s^{*+}f_2$	T	$385^{+203+31+52}_{-156-44-48}$	207	167	$25^{+1.1+0.7}_{-0.8-0.8}$
$B^+ \rightarrow D_s^{*+}f_2'$	A	$21.6^{+6.77+1.00+3.00}_{-6.03-2.32-2.70}$	4.0	2.0	$83^{+5.2+1.9}_{-5.3-1.9}$
$B^+ \rightarrow D_s^{*+}\bar{K}_2^{*0}$	A	$1.25^{+0.36+0.06+0.16}_{-0.34-0.16-0.15}$	...	...	$81^{+1.6+3.7}_{-1.8-3.3}$
$B_s \rightarrow D^{*0}a_2^0$	E	$2.68^{+0.91+0.70+0.37}_{-0.81-0.63-0.33}$	...	...	$21^{+2.6+4.8}_{-3.0-3.9}$
$B_s \rightarrow D^{*0}f_2$	E	$5.06^{+1.93+0.84+0.71}_{-1.65-0.98-0.62}$	0.24	...	$14^{+2.0+2.0}_{-2.1-1.6}$
$B_s \rightarrow D^{*0}f_2'$	C	$36.2^{+17.3+5.62+4.90}_{-14.4-5.51-4.60}$	16	...	$17^{+2.9+1.6}_{-3.1-1.1}$
$B_s \rightarrow D^{*0}\bar{K}_2^{*0}$	C	$2.06^{+1.03+0.33+0.25}_{-0.83-0.31-0.24}$	0.7	...	$21^{+3.0+0.8}_{-3.6-0.6}$
$B_s \rightarrow D^{*+}a_2^-$	E	$5.36^{+1.82+1.41+0.74}_{-1.59-1.27-0.66}$	...	...	$21^{+2.6+4.8}_{-3.0-3.9}$
$B_s \rightarrow D^{*+}K_2^{*-}$	T	$14.8^{+7.42+0.90+1.94}_{-5.93-0.85-1.77}$	12	...	$26^{+1.2-0.1}_{-1.0-0.2}$
$B_s \rightarrow D_s^{*+}K_2^{*-}$	T	$332^{+172+20+46}_{-138-31-41}$	261	...	$34^{+1.9+1.5}_{-1.6-1.0}$

ratios for the considered decay modes are summarized in Tables I– IV. We also show the results from ISGW II model [14, 15] in these tables for comparison if applicable. For those decays with a tensor meson emitted and most of the pure annihilation type decays, our results are the first time theoretical predictions. For the theoretical uncertainties, we estimate three kinds of them: The first errors are caused by the hadronic parameters, such as the decay constants and the shape parameters in wave functions of charmed meson and

TABLE III: Branching ratios of  $B_{(s)} \rightarrow \bar{D}T$  decays calculated in the PQCD approach together with results from ISGW II model [14, 15] (unit:  $10^{-5}$ ).

Decay Modes	Class	This Work	SDV[14]	KLO[15]
$B^0 \rightarrow \bar{D}^0 a_2^0$	C	$12.3^{+3.21+3.08+0.67}_{-2.99-3.24-0.40}$	8.2	4.8
$B^0 \rightarrow \bar{D}^0 f_2$	C	$9.46^{+2.52+3.64+0.51}_{-2.29-3.73-0.32}$	8.8	5.3
$B^0 \rightarrow \bar{D}^0 f_2'$	C	$0.18^{+0.04+0.06-0.09}_{-0.05-0.07-0.06}$	0.17	0.062
$B^0 \rightarrow \bar{D}^0 K_2^{*0}$	C	$1.45^{+0.41+0.29-0.09}_{-0.38-0.33-0.05}$	0.81	0.68
$B^0 \rightarrow D^- a_2^+$	T	$39.8^{+15.3+12.5+2.15}_{-12.6-12.1-1.34}$	...	...
$B^0 \rightarrow D^- K_2^{*+}$	T	$1.16^{+0.50+0.52+0.06}_{-0.40-0.47-0.05}$	...	...
$B^0 \rightarrow D_s^- K_2^{*+}$	E	$6.06^{+1.73+0.43+0.32}_{-1.65-1.04-0.21}$	...	...
$B^+ \rightarrow \bar{D}^0 a_2^+$	T,C	$41.5^{+16.5+13.0+2.24}_{-12.6-14.2-1.40}$	18	10
$B^+ \rightarrow \bar{D}^0 K_2^{*+}$	T,C	$3.33^{+1.33+0.87+0.20}_{-1.02-0.91-0.13}$	0.87	0.73
$B_s \rightarrow \bar{D}^0 a_2^0$	E	$0.11^{+0.04+0.01+0.01}_{-0.04-0.02-0.01}$	...	...
$B_s \rightarrow \bar{D}^0 f_2$	E	$0.14^{+0.04+0.01+0.01}_{-0.05-0.03-0.01}$	0.0099	...
$B_s \rightarrow \bar{D}^0 f_2'$	C	$1.36^{+0.53+0.22+0.08}_{-0.43-0.26-0.06}$	0.67	...
$B_s \rightarrow \bar{D}^0 \bar{K}_2^{*0}$	C	$20.3^{+7.70+3.98+1.00}_{-6.41-4.59-0.80}$	11	...
$B_s \rightarrow D^- a_2^+$	E	$0.23^{+0.08+0.02+0.01}_{-0.08-0.04-0.01}$	...	...
$B_s \rightarrow D_s^- a_2^+$	T	$11.3^{+5.53+6.11+0.61}_{-4.43-4.88-0.38}$	...	...
$B_s \rightarrow D_s^- K_2^{*+}$	T,E	$1.97^{+0.81+0.72+0.12}_{-0.69-0.67-0.08}$	...	...

the  $B_{(s)}$  meson, which are given in Sec. II, and the decay constants of tensor mesons given in Appendix A. The second errors are estimated from the unknown next-to-leading order QCD corrections with respect to  $\alpha_s$  and nonperturbative power corrections with respect to scales in Sudakov exponents, characterized by the choice of the  $\Lambda_{QCD} = (0.25 \pm 0.05)$  GeV and the variations of the factorization scales shown in Appendix A. The third error is from the uncertainties of the CKM matrix elements. It is easy to see that the most important theoretical uncertainty is caused by the non-perturbative hadronic parameters, which can be improved by later experiments.

As we know that all these decays do not have contributions from the penguin operators. There are only four types of topology diagrams: the color allowed diagrams (T), the color suppressed diagrams (C), the W annihilation diagrams (A) and the W exchange diagrams (E). All decays are thus classified in the tables according to their dominant contribution. Compared with  $B \rightarrow D^{(*)}T$  decays, the  $B \rightarrow \bar{D}^{(*)}T$  decays are enhanced by the CKM matrix elements  $|V_{cb}/V_{ub}|^2$ , especially for those without a strange quark in the four-quark



TABLE IV: Branching ratios (unit: $10^{-5}$ ) and the percentage of transverse polarizations  $R_T$ (unit:%) of  $B_{(s)} \rightarrow \bar{D}^* T$  decays calculated in PQCD approach together with results from ISGW II model [14, 15].

Decay Modes	Class	Branching Ratio			$R_T$
		This Work	SDV[14]	KLO[15]	
$B^0 \rightarrow \bar{D}^{*0} a_2^0$	C	$39.3^{+13.6+2.05+2.15}_{-11.1-0.50-1.34}$	12	7.8	$73^{+4.6+9.0}_{-4.3-8.1}$
$B^0 \rightarrow \bar{D}^{*0} f_2$	C	$38.2^{+13.9+1.97+2.10}_{-11.6-1.22-1.30}$	13	8.4	$70^{+5.9+9.4}_{-5.6-6.3}$
$B^0 \rightarrow \bar{D}^{*0} f_2'$	C	$0.72^{+0.26+0.02+0.04}_{-0.22-0.03-0.03}$	0.26	0.11	$70^{+5.9+9.4}_{-5.6-6.3}$
$B^0 \rightarrow \bar{D}^{*0} K_2^{*0}$	C	$5.32^{+1.69+0.79+0.32}_{-1.42-0.66-0.22}$	1.3	1.1	$71^{+1.8+8.6}_{-1.6-8.8}$
$B^0 \rightarrow D^{*-} a_2^+$	T	$29.6^{+11.5+9.58+1.62}_{-9.86-10.1-1.01}$	...	...	$3^{+0.2+0.4}_{-0.2-0.4}$
$B^0 \rightarrow D^{*-} K_2^{*+}$	T	$1.15^{+0.49+0.46+0.07}_{-0.37-0.43-0.04}$	...	...	$7^{+0.4+0.3}_{-0.2-0.3}$
$B^0 \rightarrow D_s^{*-} K_2^{*+}$	E	$4.55^{+1.32+0.48+0.25}_{-1.14-0.51-0.16}$	...	...	$22^{+3.0+7.6}_{-3.4-6.7}$
$B^+ \rightarrow \bar{D}^{*0} a_2^+$	T,C	$80.6^{+29.0+3.67+4.41}_{-24.1-3.12-2.75}$	26	17	$58^{+3.7+13.8}_{-3.2-10.2}$
$B^+ \rightarrow \bar{D}^{*0} K_2^{*+}$	T,C	$6.81^{+2.36+0.34+0.42}_{-1.93-0.30-0.27}$	1.4	1.2	$57^{+1.4+14.1}_{-1.3-11.6}$
$B_s \rightarrow \bar{D}^{*0} a_2^0$	E	$0.09^{+0.03+0.01+0.01}_{-0.03-0.01-0.01}$	...	...	$26^{+4.0+6.5}_{-4.4-6.8}$
$B_s \rightarrow \bar{D}^{*0} f_2$	E	$0.21^{+0.08+0.01+0.01}_{-0.07-0.02-0.01}$	0.016	...	$11^{+0.6+2.2}_{-0.6-1.0}$
$B_s \rightarrow \bar{D}^{*0} f_2'$	C	$5.02^{+2.06+0.39+0.30}_{-1.70-0.50-0.20}$	1.1	...	$71^{+1.1+7.5}_{-1.0-7.2}$
$B_s \rightarrow \bar{D}^{*0} \bar{K}^{*0}$	C	$70.1^{+28.8+4.10+3.83}_{-23.9-5.82-2.40}$	17	...	$68^{+1.7+8.5}_{-1.3-7.9}$
$B_s \rightarrow D^{*-} a_2^+$	E	$0.18^{+0.06+0.01+0.01}_{-0.06-0.03-0.01}$	...	...	$26^{+4.0+6.5}_{-4.4-6.8}$
$B_s \rightarrow D_s^{*-} a_2^+$	T	$11.5^{+5.59+5.79+0.63}_{-4.44-4.70-0.40}$	...	...	$6^{+0.1+0.2}_{-0.1-0.3}$
$B_s \rightarrow D_s^{*-} K_2^{*+}$	T,E	$1.73^{+0.75+0.65+0.11}_{-0.60-0.58-0.06}$	...	...	$11^{+0.9+2.3}_{-0.9-2.4}$

operators. So for most of the  $B \rightarrow D^{(*)}T$  decays, the branching ratios are at the order  $10^{-6}$  or  $10^{-7}$ ; while for the  $B \rightarrow \bar{D}^{(*)}T$  decays, the branching ratios are at the order  $10^{-4}$  or  $10^{-5}$ .

As usual, the nonfactorizable emission diagrams with a light meson emitted are suppressed, because the contributions from two diagrams cancel with each other. However, when the emitted meson is the  $D(\bar{D})$  or tensor meson, the situation is changed. Unlike the light meson, the difference between  $c(\bar{c})$  quark and the light quark is very big in the heavy  $D(\bar{D})$  meson [34, 35]. The nonfactorizable diagrams also provide non-negligible contributions. When the tensor meson is emitted, the contributions from two nonfactorizable diagrams shown in Fig.3 strengthen with each other, because the wave function of tensor meson is antisymmetric under the interchange of the momentum fractions of the quark and antiquark [8, 9]. Since the factorizable emission diagrams with a tensor

meson emitted are prohibited, the contribution of nonfactorizable emission diagrams play the decisive role. For these color suppressed decay channels, since the factorizable contribution is suppressed by the Wilson coefficient  $a_2$  ( $C_1 + C_2/3$ )  $\simeq 0.1$ , while the Wilson coefficient for nonfactorizable contribution is  $C_2 \simeq 1.0$ , the nonfactorizable contribution plays the crucial role in the amplitude. From table I to IV, one can see that for the color suppressed decay modes, the predicted branching ratios in the PQCD approach are larger than those of Ref.[14] and Ref.[15]. For  $B^0 \rightarrow \bar{D}^0 f_2$ , our predicted branching ratio  $\mathcal{B}(B^0 \rightarrow \bar{D}^0 f_2) = 9.46 \times 10^{-5}$ , which is larger than other approaches, agrees better with the experimental data  $(12 \pm 4) \times 10^{-5}$  [1]. In addition, the annihilation diagrams can also provide relatively sizable contributions. Our results show that the contributions from annihilation diagrams are even at the same order as the emission diagrams in some decay modes. Some of the pure annihilation type decays are already discussed in Ref. [17] with large branching ratios.

For those color allowed decay channels, the Wilson coefficient for factorizable contribution is  $a_1 = (C_1/3 + C_2) \simeq 1$ , while for the nonfactorizable contribution is  $C_1 \simeq -0.3$ . The contribution of nonfactorizable diagrams is highly suppressed by the Wilson coefficient. The decay amplitude is dominated by the contribution from factorizable emission diagrams, which can be naively factorized as the product of the Wilson coefficient  $a_1$ , the decay constant of  $D$  meson and the  $B$  to tensor meson form factor. In this case, our predicted branching ratios basically agree with the predictions of naive factorization approach in Ref.[14]. The small difference is caused by parameter changes and the interference from nonfactorizable and annihilation diagrams. For those decays with a tensor meson emitted, for example,  $B^0 \rightarrow D^- a_2^+$ , since the factorizable emission diagrams are prohibited, the predictions can not be given within the naive factorization framework. But these decays can get contributions from nonfactorizable and annihilation type diagrams, which can be calculated in the PQCD approach. The branching ratios of these decays are predicted for the first time in table I-IV.

Similar to the relation  $\mathcal{B}(B^0 \rightarrow \bar{D}^{(*)0} \rho^0) > \mathcal{B}(B^0 \rightarrow \bar{D}^{(*)0} \omega)$  [22], we also get  $\mathcal{B}(B^0 \rightarrow \bar{D}^{(*)0} a_2^0) > \mathcal{B}(B^0 \rightarrow \bar{D}^{(*)0} f_2)$ . This can be explained by the interference between contributions from emission diagram (C) and contributions from annihilation diagrams (E). The interference can also explain why  $\mathcal{B}(B^+ \rightarrow D^{(*)+} f_2) > \mathcal{B}(B^+ \rightarrow D^{(*)+} a_2^0)$ . The relative sign of the annihilation diagrams (A) with respect to the emission diagrams (T)

is negative for the  $a_2$  meson and positive for  $f_2$  meson. The interference is constructive for  $B^+ \rightarrow D^{(*)+} f_2$ , while destructive for  $B^+ \rightarrow D^{(*)+} a_2^0$ .

For decays involving  $f_2^{(\prime)}$  in the final states, for example,  $B^0 \rightarrow D^0 f_2^{(\prime)}$ , there are no contributions from  $s\bar{s}$  component. The branching ratios have the simple relation derived from Eq.(A1):

$$r = \frac{\mathcal{B}(B \rightarrow D f_2')}{\mathcal{B}(B \rightarrow D f_2)} = \frac{\sin^2 \theta}{\cos^2 \theta}. \quad (62)$$

This provides a potential way to measure the mixing angle of  $f_2$  and  $f_2'$ , for example,  $r \simeq 0.02$  with  $\theta = 7.8^\circ$ .

For  $B \rightarrow D^*(\bar{D}^*)T$  decays, we also calculate the percentage of transverse polarizations

$$R_T = \frac{\mathcal{A}_+^2 + \mathcal{A}_-^2}{\mathcal{A}_0^2 + \mathcal{A}_+^2 + \mathcal{A}_-^2}. \quad (63)$$

The numerical results shown in table II and IV are only indicative, because the transversely polarized contributions are suppressed by  $r_T$  or  $r_{D^*}$  to make it more sensitive to meson wave function parameters and higher order corrections [34]. According to the power counting rules in the factorization assumption, the longitudinal polarization should be dominant due to the quark helicity analysis [39, 40]. This is true for those color favored decay channels, such as  $B^0 \rightarrow D^{*-} a_2^+$ ,  $B^0 \rightarrow D^{*-} K_2^{*+}$ ,  $B_s^0 \rightarrow D_s^{*-} a_2^+$ ,  $B_s^0 \rightarrow D_s^{*-} K_2^{*+}$ .

However, for those color suppressed (C)  $B \rightarrow \bar{D}^* T$  ( $\bar{b} \rightarrow \bar{c}$  transition) decays with the  $\bar{D}^*$  emitted, the percentage of transverse polarizations are about 70%, while for color suppressed (C)  $B \rightarrow D^* T$  ( $\bar{b} \rightarrow \bar{u}$  transition) decays with  $D^*$  meson emitted, the percentage of transverse polarizations are only at the range of 20% to 30%. For  $B \rightarrow \bar{D}^* T$  decays, we know that the  $\bar{c}$  quark and the  $u$  quark in  $\bar{D}^*$  meson produced through  $(V-A)$  current are right-handed and left-handed respectively. So the  $\bar{D}^*$  meson is longitudinally polarized. But the helicity of  $\bar{c}$  quark can flip easily from right handed to left handed, because the  $\bar{c}$  quark is massive. Therefore the  $\bar{D}^*$  can be transversely polarized with the polarization  $\lambda = -1$ . The recoiled tensor meson can also be transversely polarized with polarization  $\lambda = -1$  due to the contribution of orbital angular momentum. Thus, the transversely polarized contribution can be sizable. For  $B \rightarrow D^* T$  decays, the emitted  $D^*$  meson can also be transversely polarized, but the polarization is  $\lambda = +1$ . The reason is that the  $\bar{u}$  quark in  $D^*$  meson is right handed, while the  $c$  quark can flip from left handed to right handed to make a  $D^*$  meson with  $\lambda = +1$ . The recoiled transversely polarized tensor

meson with polarization  $\lambda = +1$  needs contributions from both orbital angular momentum and spin, so the situation is symmetric. But the wave function of tensor meson is asymmetric. Therefore the transversely polarized contribution is suppressed, because of Bose statistics.

As discussed in Ref.[35], the W annihilation diagrams give a very large contribution of transverse polarizations. In our calculations, we also find very large transverse polarizations up to 80% for the W annihilation (A) type  $B \rightarrow D^*T$  decays, such as  $B^+ \rightarrow D^{*+}K_2^{*0}$ ,  $B^+ \rightarrow D_s^{*+}\bar{K}_2^{*0}$  and  $B^+ \rightarrow D_s^{*+}f_2'$  decays. This can be understood as following [41]: For the  $D^*$  meson, the “light quark-anti-quark” pair created from hard gluon are left-handed or right-handed with equal opportunity. So the  $D^*$  meson can be longitudinally polarized or transversely polarized with polarization  $\lambda = -1$ . For the tensor meson, the anti-quark from four quark operator is right-handed, and the quark produced from hard gluon can be either left-handed or right-handed. So the tensor meson can be longitudinally polarized or transversely polarized with polarization  $\lambda = -1$ , because of the additional contribution from the orbital angular momentum. So the transverse polarization can become so large with additional interference from other diagrams. Although annihilation type diagrams, the W exchange diagrams (E) contribute little to transverse polarizations, which is consistent with the argument in  $B \rightarrow D^*V$  decays [34, 35]. Examples are  $B_s \rightarrow D^{*0}a_2^0$ ,  $B_s \rightarrow \bar{D}^{*0}a_2^0$ ,  $B_s \rightarrow D^{*0}f_2$ ,  $B_s \rightarrow \bar{D}^{*0}f_2$ ,  $B_s \rightarrow D^{*+}a_2^-$ ,  $B_s \rightarrow D^{*-}a_2^+$ ,  $B^0 \rightarrow D_s^{*+}K_2^{*-}$ ,  $B^0 \rightarrow D_s^{*-}K_2^{*+}$ , with only 10-20% transverse polarization contributions.

## V. SUMMARY

In this paper, we investigate the  $B_{(s)} \rightarrow D^{(*)}T, \bar{D}^{(*)}T$  decays within the framework of perturbative QCD approach. We calculate the contributions of different diagrams in the leading order approximation of  $m_D/m_B$  expansion. We find that the nonfactorizable and annihilation type diagrams provide large contributions, especially for those color suppressed channels and the decays with a tensor meson emitted. We predict the branching ratios and the ratios of the transverse polarized contributions and find that the branching ratios for  $B_{(s)} \rightarrow D^{(*)}T$  decays are in the range of  $10^{-5}$  to  $10^{-8}$ , while  $10^{-4}$  to  $10^{-6}$  for  $B_{(s)} \rightarrow \bar{D}^{(*)}T$  decays. For those color suppressed  $B_{(s)} \rightarrow \bar{D}^{(*)}T$  decays, the transversely polarized contributions from nonfactorizable diagrams are very large. For those W anni-

hilation type  $B \rightarrow D^*T$  decays, the transverse polarized contributions from factorizable annihilation diagrams are as large as 80%.

### Acknowledgment

We are very grateful to Xin Liu and Run-Hui Li for helpful discussions. This Work is partly supported by the National Science Foundation of China under the Grant No.11075168.

### Appendix A: Input Parameters and Hard Functions

TABLE V: The masses and decay constants of light tensor mesons [8, 42, 43]

Tensor(mass(MeV))	$f_T(\text{MeV})$	$f_T^\perp(\text{MeV})$
$f_2(1270)$	$102 \pm 6$	$117 \pm 25$
$f_2'(1525)$	$126 \pm 4$	$65 \pm 12$
$a_2(1320)$	$107 \pm 6$	$105 \pm 21$
$K_2^*(1430)$	$118 \pm 5$	$77 \pm 14$

The masses and decay constants of tensor mesons are summarized in Table V. Other parameters such as QCD scale  $\Lambda_{\overline{MS}}^{f=4} = 0.25 \text{ GeV}$  and the b quark mass  $m_b = 4.8(\text{GeV})$ . For the CKM matrix elements, here we adopt the Wolfenstein parameterization  $A = 0.808$ ,  $\lambda = 0.2253$ ,  $\bar{\rho} = 0.132$  and  $\bar{\eta} = 0.341$  [1].

Like the  $\eta - \eta'$  mixing, the iso-singlet tensor meson states  $f_2(1270)$  and  $f_2'(1525)$  are also a mixture of  $f_2^q = \frac{1}{\sqrt{2}}(u\bar{u} + d\bar{d})$  and  $f_2^s = s\bar{s}$

$$\begin{aligned} f_2 &= f_2^q \cos \theta + f_2^s \sin \theta, \\ f_2' &= f_2^q \sin \theta - f_2^s \cos \theta, \end{aligned} \tag{A1}$$

with the mixing angle  $\theta = 5.8^\circ$  [44],  $7.8^\circ$  [45] or  $(9 \pm 1)^\circ$  [1].

The functions  $h$  in the decay amplitudes consist of two parts: the jet function  $S_t(x_i)$  and the propagator of virtual quark and gluon. The former is gained by the threshold re-summation [26]. For factorizable emission diagrams Fig.1. 1a and 1b, the  $h$  function

can be given by

$$\begin{aligned}
h_{ef}(x_1, x_3, b_1, b_3) &= K_0(\sqrt{x_1 x_3} m_B b_1) \\
&\times \{ \theta b_1 - b_3 K_0(\sqrt{x_3} m_B b_1) I_0(\sqrt{x_3} m_B b_3) \\
&+ \theta(b_3 - b_1) K_0(\sqrt{x_3} m_B b_3) I_0(\sqrt{x_3} m_B b_1) \} \\
&\times S_t(x_3).
\end{aligned} \tag{A2}$$

The hard scales are determined by

$$\begin{aligned}
t_a &= \max\{\sqrt{x_3(1 - r_D^2)} m_B, 1/b_1, 1/b_3\}, \\
t_b &= \max\{\sqrt{x_1(1 - r_D^2)} m_B, 1/b_1, 1/b_3\}.
\end{aligned} \tag{A3}$$

Jet function appears in the factorization formulae is [26]

$$S_t(x) = \frac{2^{1+2c} \Gamma(3/2 + c)}{\sqrt{\pi} \Gamma(1 + c)} [x(1 - x)]^c, \tag{A4}$$

where  $c = 0.5$ . For the nonfactorizable diagrams, we omit the  $S_t(x)$ , because it provides a very small numerical effect to the amplitude [46].

The evolution factors  $E_{ef}(t_a)$  and  $E_{ef}(t_b)$  in the matrix elements (see section III) are given by

$$E_{ef}(t) = \alpha_s(t) \exp[-S_B(t) - S_T(t)]. \tag{A5}$$

The Sudakov exponents are defined as

$$S_B(t) = s\left(x_1 \frac{m_B}{\sqrt{2}}, b_1\right) + \frac{5}{3} \int_{1/b_1}^t \frac{d\bar{\mu}}{\bar{\mu}} \gamma_q(\alpha_s(\bar{\mu})), \tag{A6}$$

$$S_D(t) = s\left(x_D \frac{m_B}{\sqrt{2}}, b\right) + 2 \int_{1/b}^t \frac{d\bar{\mu}}{\bar{\mu}} \gamma_q(\alpha_s(\bar{\mu})), \tag{A7}$$

$$S_T(t) = s\left(x_T \frac{m_B}{\sqrt{2}}, b\right) + s\left((1 - x_T) \frac{m_B}{\sqrt{2}}, b\right) + 2 \int_{1/b}^t \frac{d\bar{\mu}}{\bar{\mu}} \gamma_q(\alpha_s(\bar{\mu})), \tag{A8}$$

where the  $s(Q, b)$  can be found in the Appendix A in the Ref.[19].  $x_{T(D)}$  is the momentum fraction of “(light) quark” in tensor (D) meson.

For the rest of diagrams, the related functions are summarized as follows:

$$\begin{aligned}
t_c &= \max\{\sqrt{x_1 x_3 (1 - r_D^2)} m_B, \sqrt{|x_1 - x_2| x_3 (1 - r_D^2)} m_B, 1/b_1, 1/b_2\}, \\
t_d &= \max\{\sqrt{x_1 x_3 (1 - r_D^2)} m_B, \sqrt{|x_1 + x_2 - 1| (r_D^2 + x_3 (1 - r_D^2)) + r_D^2} m_B, \\
&1/b_1, 1/b_2\},
\end{aligned} \tag{A9}$$

$$E_{enf}(t) = \alpha_s(t) \cdot \exp[-S_B(t) - S_D(t) - S_T(t)] \mid_{b_1=b_3}, \quad (\text{A10})$$

$$\begin{aligned} h_{enfj}(x_1, x_2, x_3, b_1, b_2) = & \left[ \theta(b_2 - b_1) K_0(\sqrt{x_1 x_3 (1 - r_D^2)} m_B b_2) I_0(\sqrt{x_1 x_3 (1 - r_D^2)} m_B b_1) \right. \\ & \left. + \theta(b_1 - b_2) K_0(\sqrt{x_1 x_3 (1 - r_D^2)} m_B b_1) I_0(\sqrt{x_1 x_3 (1 - r_D^2)} m_B b_2) \right] \\ & \cdot \begin{cases} \frac{i\pi}{2} H_0^{(1)} \left( \sqrt{|D_j^2|} m_B b_2 \right), & D_j^2 < 0; \\ K_0(D_j m_B b_2), & D_j^2 > 0, \end{cases} \end{aligned} \quad (\text{A11})$$

with  $j = 1, 2$  and  $H_0^{(1)}(z) = J_0(z) + iY_0(z)$ .

$$\begin{aligned} D_1^2 &= (x_1 - x_2) x_3 (1 - r_D^2) m_B^2, \\ D_2^2 &= (x_1 + x_2 - 1)(r_D^2 + x_3(1 - r_D^2)) + r_D^2. \end{aligned} \quad (\text{A12})$$

$$\begin{aligned} t_e &= \max\{\sqrt{x_3(1 - r_D^2)} m_B, 1/b_2, 1/b_3\}, \\ t_f &= \max\{\sqrt{x_2(1 - r_D^2)} m_B, 1/b_2, 1/b_3\}, \end{aligned} \quad (\text{A13})$$

$$E_{af}(t) = \alpha_s(t) \cdot \exp[-S_T(t) - S_D(t)], \quad (\text{A14})$$

$$\begin{aligned} h_{af}(x_2, x_3, b_2, b_3) &= \left( \frac{i\pi}{2} \right)^2 H_0^{(1)}(\sqrt{x_2 x_3} m_B b_2) \\ & \left[ \theta(b_2 - b_3) H_0^{(1)}(\sqrt{x_3} m_B b_2) J_0(\sqrt{x_3} m_B b_3) + \right. \\ & \left. \theta(b_3 - b_2) H_0^{(1)}(\sqrt{x_3} m_B b_3) J_0(\sqrt{x_3} m_B b_2) \right] \cdot S_t(x_3). \end{aligned} \quad (\text{A15})$$

$$\begin{aligned} t_g &= \max\{\sqrt{x_2 x_3 (1 - r_D^2)} m_B, \sqrt{1 - (1 - x_3)(1 - x_1 - x_2(1 - r_D^2))} m_B, \\ & \quad 1/b_1, 1/b_2\}, \\ t_h &= \max\{\sqrt{x_2 x_3 (1 - r_D^2)} m_B, \sqrt{x_3 |x_1 - x_2(1 - r_D^2)|} m_B, 1/b_1, 1/b_2\}, \end{aligned} \quad (\text{A16})$$

$$E_{anf} = \alpha_s(t) \cdot \exp[-S_B(t) - S_T(t) - S_D(t)] \mid_{b_2=b_3}, \quad (\text{A17})$$

$$\begin{aligned} h_{anfj}(x_1, x_2, x_3, b_1, b_2) &= \frac{i\pi}{2} \left[ \theta(b_1 - b_2) H_0^{(1)}(F m_B b_1) J_0(F m_B b_2) \right. \\ & \quad \left. + \theta(b_2 - b_1) H_0^{(1)}(F m_B b_2) J_0(F m_B b_1) \right] \\ & \quad \times \begin{cases} \frac{i\pi}{2} H_0^{(1)} \left( \sqrt{|F_j^2|} m_B b_1 \right), & F_j^2 < 0, \\ K_0(F_j m_B b_1), & F_j^2 > 0, \end{cases} \end{aligned} \quad (\text{A18})$$

with  $j = 1, 2$ .

$$\begin{aligned}
F^2 &= x_2 x_3 (1 - r_D^2), \\
F_1^2 &= 1 - (1 - x_3)(1 - x_1 - x_2(1 - r_D^2)), \\
F_2^2 &= x_3(x_1 - x_2(1 - r_D^2)).
\end{aligned} \tag{A19}$$

For  $B \rightarrow \bar{D}^{(*)}T$  decays:

$$\begin{aligned}
t'_{e(f)} &= t_{e(f)}(x_2 \rightarrow 1 - x_3, x_3 \rightarrow x_2), \\
h'_{anfj} &= h_{anfj}(x_3 \rightarrow (1 - x_3)(1 - r_D^2), x_2(1 - r_D^2) \rightarrow x_2), \\
t'_{g(h)} &= t_{g(h)}(x_3 \rightarrow (1 - x_3)(1 - r_D^2), x_2(1 - r_D^2) \rightarrow x_2),
\end{aligned} \tag{A20}$$

$$\begin{aligned}
t_c^3 &= \max\{\sqrt{x_1 x_3} m_B, \sqrt{|x_1 - (1 - x_2)(1 - r_D^2)| x_3} m_B, 1/b_1, 1/b_2\}, \\
t_d^3 &= \max\{\sqrt{x_1 x_3} m_B, \sqrt{|x_1 - x_2(1 - r_D^2)| x_3} m_B, 1/b_1, 1/b_2\},
\end{aligned} \tag{A21}$$

$$\begin{aligned}
E_{enf}^3(x_1, x_2, x_3, b_1, b_2) &= [\theta(b_2 - b_1) I_0(\sqrt{x_1 x_3} m_B b_1) K_0(\sqrt{x_1 x_3} m_B b_2) \\
&\quad + \theta(b_1 - b_2) I_0(\sqrt{x_1 x_3} m_B b_2) K_0(\sqrt{x_1 x_3} m_B b_1)] \\
&\quad \times \begin{cases} \frac{i\pi}{2} H_0^{(1)}(\sqrt{|G^2|} m_B b_2), & G^2 < 0, \\ K_0(G m_B b_2), & G^2 > 0, \end{cases}
\end{aligned} \tag{A22}$$

with  $G^2 = (x_1 - x_2(1 - r_D^2))x_3 m_B^2$ .

## Appendix B: Formulas for $B \rightarrow \bar{D}^{(*)}T$ decay Amplitudes

For  $B \rightarrow \bar{D}T$  decays, the expression of the factorizable emission contributions ( $\mathcal{A}_{ef}$ ) is the same as Eq.(18). For nonfactorizable emission diagrams, the amplitudes are given by

$$\begin{aligned}
\mathcal{M}_{enf} &= -\frac{32}{3} C_F \pi m_B^4 \int_0^1 dx_1 dx_2 dx_3 \int_0^{1/\Lambda} b_1 db_1 b_2 db_2 \phi_B(x_1, b_1) \phi_D(x_2, b_2) \\
&\quad \times \{ [\phi_T(x_3)(1 - x_2) + (\phi_T^t(x_3) - \phi_T^s(x_3)) r_T x_3] \\
&\quad \cdot h_{enf2}(x_i, b_i) E_{enf}(t_d) \\
&\quad + [-\phi_T(x_3)(x_2 + x_3) + (\phi_T^s(x_3) + \phi_T^t(x_3)) r_T x_3] \\
&\quad \cdot h_{enf1}(x_i, b_i) E_{enf}(t_c) \}.
\end{aligned} \tag{B1}$$



The decay amplitudes of factorizable annihilation contributions ( $\mathcal{A}_{af}$ ) can be obtain by making the following substitutions in Eq.(20),

$$x_2 \rightarrow 1 - x_3, \quad x_3 \rightarrow x_2, \quad \phi_T^{(t,s)}(x_2) \rightarrow \phi_T^{(t,s)}(1 - x_3), \quad \phi_D(x_3, b_3) \rightarrow \phi_D(x_2, b_2). \quad (\text{B2})$$

While for the non-factorizable annihilation contributions, the decay amplitude is

$$\begin{aligned} \mathcal{M}_{anf} = & \frac{32}{3} C_F \pi m_B^4 \int_0^1 dx_1 dx_2 dx_3 \int_0^{1/\Lambda} b_1 db_1 b_2 db_2 \phi_B(x_1, b_1) \phi_D(x_2, b_2) \\ & \times \left\{ [\phi_T(x_3)x_2 + r_D r_T (\phi_T^s(x_3)(x_3 - x_2 - 3) + \phi_T^t(x_3)(x_2 + x_3 - 1))] \right. \\ & \cdot h'_{anf1}(x_1, x_2, x_3, b_1, b_2) E_{anf}(t'_g) \\ & + [\phi_T(x_3)(x_3 - 1) + r_D r_T (\phi_T^s(x_3)(x_2 - x_3 + 1) + \phi_T^t(x_3)(x_2 + x_3 - 1))] \\ & \cdot h'_{anf2}(x_1, x_2, x_3, b_1, b_2) E_{anf}(t'_h) \left. \right\}. \end{aligned} \quad (\text{B3})$$

For those two nonfactorizable emission diagrams in Fig.3, the decay amplitude is

$$\begin{aligned} \mathcal{M}_{enf}^3 = & \frac{32}{3} C_F \pi m_B^4 \int_0^1 dx_1 dx_2 dx_3 \int_0^{1/\Lambda} b_1 db_1 b_2 db_2 \phi_B(x_1, b_1) \phi_D(x_3, b_1) \\ & \times \left\{ [\phi_T(x_2)(x_2 - 1 + r_D x_3)] h_{enf}^3(x_1, (1 - x_2), x_3, b_1, b_2) E_{enf}(t_c^3) \right. \\ & + [\phi_T(x_2)(x_2 + x_3 - r_D x_3)] h_{enf}^3(x_1, x_2, x_3, b_1, b_2) E_{enf}(t_d^3) \left. \right\}. \end{aligned} \quad (\text{B4})$$

For  $B \rightarrow \bar{D}^* T$  decays, the expressions of the longitudinally polarized contributions of the emission diagrams can be obtained from those corresponding  $B \rightarrow \bar{D} T$  decays by substitution in Eq.23. For the annihilation type diagrams, the decay amplitudes are

$$\begin{aligned} \mathcal{A}_{af}^L = & 8\sqrt{\frac{2}{3}} C_F f_B \pi m_B^4 \int_0^1 dx_2 dx_3 \int_0^{1/\Lambda} b_2 db_2 b_3 db_3 \phi_D^L(x_2, b_2) \\ & \times \left\{ [\phi_T(x_3)(1 - x_3) - r_D r_T (\phi_T^s(x_3) + \phi_T^t(x_3))] \right. \\ & \cdot h_{af}(1 - x_3, x_2(1 - r_D^2), b_2, b_3) E_{af}(t'_e) \\ & + [-\phi_T(x_3)x_2 + 2r_D r_T \phi_T^s(x_3)(x_2 - 1)] \\ & \cdot h_{af}(x_2, (1 - x_3)(1 - r_D^2), b_3, b_2) E_{af}(t'_f) \left. \right\}, \end{aligned} \quad (\text{B5})$$

$$\begin{aligned} \mathcal{M}_{anf}^L = & \frac{32}{3} C_F \pi m_B^4 \int_0^1 dx_1 dx_2 dx_3 \int_0^{1/\Lambda} b_1 db_1 b_2 db_2 \phi_B(x_1, b_1) \phi_D^L(x_2, b_2) \\ & \times \left\{ [\phi_T(x_3)x_2 - r_D r_T (\phi_T^t(x_3)(1 + x_3 - x_2) + \phi_T^s(x_3)(x_2 + x_3 - 1))] \right. \\ & \cdot h'_{anf1}(x_1, x_2, x_3, b_1, b_2) E_{anf}(t'_g) \\ & + [\phi_T(x_3)(x_3 - 1) - r_D r_T (\phi_T^t(x_3)(x_2 - x_3 + 1) + \phi_T^s(x_3)(x_2 + x_3 - 1))] \\ & \cdot h'_{anf2}(x_1, x_2, x_3, b_1, b_2) E_{anf}(t'_h) \left. \right\}. \end{aligned} \quad (\text{B6})$$

The transversely polarized contributions are suppressed by  $r_D$  or  $r_T$ . For the factorizable emission diagrams, the expressions are the same as Eq.(26) and Eq.(27). For the non-factorizable emission diagrams, the decay amplitudes are

$$\begin{aligned}\mathcal{M}_{enf}^T = & 16\sqrt{\frac{1}{3}}C_F\pi r_D m_B^4 \int_0^1 dx_1 dx_2 dx_3 \int_0^{1/\Lambda} b_1 db_1 b_2 db_2 \phi_B(x_1, b_1) \phi_D^T(x_2, b_2) \\ & \times \left\{ [\phi_T^T(x_3)(x_2 - 1) + r_T(\phi_T^a(x_3) - \phi_T^v(x_3))] h_{enf2}(x_i, b_i) E_{enf}(t_d) \right. \\ & \left. + [-\phi_T^T(x_3)x_2 + 2r_T(x_2 + x_3)\phi_T^v(x_3)] h_{enf1}(x_i, b_i) E_{enf}(t_c) \right\},\end{aligned}\quad (\text{B7})$$

$$\mathcal{M}_{enf}^N = \mathcal{M}_{enf}^T(\phi_T^a \leftrightarrow \phi_T^v). \quad (\text{B8})$$

For factorizable annihilation diagrams, the transverse decay amplitudes are

$$\begin{aligned}\mathcal{A}_{af}^T = & -4\sqrt{2}C_F f_B \pi m_B^4 r_D \int_0^1 dx_2 dx_3 \int_0^{1/\Lambda} b_2 db_2 b_3 db_3 \phi_D^T(x_2, b_2) \\ & \times \left\{ [r_D \phi_T^T(x_3) - r_T(\phi_T^a(x_3)x_3 - \phi_T^v(x_3)(x_3 - 2))] \right. \\ & \cdot h_{af}(1 - x_3, x_2(1 - r_D^2), b_2, b_3) E_{af}(t_e) \\ & + r_T [\phi_T^v(x_3)(x_2 + 1) + \phi_T^a(x_3)(x_2 - 1)] \\ & \left. \cdot h_{af}(x_2, (1 - x_3)(1 - r_D^2), b_3, b_2) E_{af}(t_f) \right\},\end{aligned}\quad (\text{B9})$$

$$\begin{aligned}\mathcal{A}_{af}^N = & -4\sqrt{2}C_F f_B \pi m_B^4 r_D \int_0^1 dx_2 dx_3 \int_0^{1/\Lambda} b_2 db_2 b_3 db_3 \phi_D^T(x_2, b_2) \\ & \times \left\{ [-r_D \phi_T^T(x_3) - r_T(\phi_T^v(x_3)x_3 - \phi_T^a(x_3)(x_3 - 2))] \right. \\ & \cdot h_{af}(1 - x_3, x_2(1 - r_D^2), b_2, b_3) E_{af}(t_e) \\ & + r_T [\phi_T^a(x_3)(x_2 + 1) + \phi_T^v(x_3)(x_2 - 1)] \\ & \left. \cdot h_{af}(x_2, (1 - x_3)(1 - r_D^2), b_3, b_2) E_{af}(t_f) \right\}.\end{aligned}\quad (\text{B10})$$

While for the non-factorizable annihilation diagrams, the transverse decay amplitudes are

$$\begin{aligned}\mathcal{M}_{anf}^T = & 16\sqrt{\frac{1}{3}}C_F\pi m_B^4 r_D \int_0^1 dx_1 dx_2 dx_3 \int_0^{1/\Lambda} b_1 db_1 b_2 db_2 \phi_B(x_1, b_1) \phi_D^T(x_2, b_2) \\ & \times \left\{ [r_D \phi_T^T(x_3)(x_2 - 1) + 2r_T \phi_T^v(x_3)] h'_{anf1}(x_1, x_2, x_3, b_1, b_2) E_{anf}(t'_g) \right. \\ & \left. - [r_D x_2 \phi_T^T(x_3)] h'_{anf2}(x_1, x_2, x_3, b_1, b_2) E_{anf}(t'_h) \right\},\end{aligned}\quad (\text{B11})$$

$$\begin{aligned}\mathcal{M}_{anf}^N = & 16\sqrt{\frac{1}{3}}C_F\pi m_B^4 r_D \int_0^1 dx_1 dx_2 dx_3 \int_0^{1/\Lambda} b_1 db_1 b_2 db_2 \phi_B(x_1, b_1) \phi_D^T(x_2, b_2) \\ & \times \left\{ [-r_D \phi_T^T(x_3)(x_2 - 1) + 2r_T \phi_T^a(x_3)] h'_{anf1}(x_1, x_2, x_3, b_1, b_2) E_{anf}(t'_g) \right. \\ & \left. + [r_D x_2 \phi_T^T(x_3)] h'_{anf2}(x_1, x_2, x_3, b_1, b_2) E_{anf}(t'_h) \right\}.\end{aligned}\quad (\text{B12})$$

The non-factorizable emission decay amplitudes for  $B \rightarrow \bar{D}^* T$  with a tensor meson emitted shown in Fig.3 are

$$\begin{aligned} \mathcal{M}_{enf}^{3L} = & -\frac{32}{3} C_F \pi m_B^4 (r_D - 1) \int_0^1 dx_1 dx_2 dx_3 \int_0^{1/\Lambda} b_1 db_1 b_2 db_2 \phi_B(x_1, b_1) \phi_D^L(x_3, b_1) \\ & \times \left\{ [\phi_T(x_2)(x_2 - 1 + r_D(x_2 - x_3 - 1))] h_{enf}^3(x_1, (1 - x_2), x_3, b_1, b_2) E_{enf}(t_c^3) \right. \\ & \left. + [\phi_T(x_2)(x_2 + x_3 + r_D x_2)] h_{enf}^3(x_1, x_2, x_3, b_1, b_2) E_{enf}(t_d^3) \right\}, \end{aligned} \quad (B13)$$

$$\begin{aligned} \mathcal{M}_{enf}^{3T} = & 16 \sqrt{\frac{1}{3}} C_F \pi m_B^4 r_T \int_0^1 dx_1 dx_2 dx_3 \int_0^{1/\Lambda} b_1 db_1 b_2 db_2 \phi_B(x_1, b_1) \phi_D^T(x_3, b_1) \\ & \times \left\{ [(\phi_T^a(x_2) + \phi_T^v(x_2))(x_2 - 1)] h_{enf}^3(x_1, (1 - x_2), x_3, b_1, b_2) E_{enf}(t_c^3) \right. \\ & + [-\phi_T^a(x_2)x_2 + \phi_T^v(x_2)((2r_D - 1)x_2 + 2r_D x_3)] \\ & \left. \cdot h_{enf}^3(x_1, x_2, x_3, b_1, b_2) E_{enf}(t_d^3) \right\}, \end{aligned} \quad (B14)$$

$$\mathcal{M}_{enf}^{3N} = -\mathcal{M}_{enf}^{3T}(\phi_T^a \leftrightarrow \phi_T^v). \quad (B15)$$

With the functions obtained in the above, the amplitudes of all  $B \rightarrow \bar{D} T$  decay channels can be given by

$$\mathcal{A}(B^0 \rightarrow \bar{D}^0 a_2^0) = \frac{G_F}{\sqrt{2}} \frac{1}{\sqrt{2}} V_{cb}^* V_{ud} [a_2 \mathcal{A}_{af} + C_2 \mathcal{M}_{anf} - a_2 \mathcal{A}_{ef} - C_2 \mathcal{M}_{enf}], \quad (B16)$$

$$\mathcal{A}(B^0 \rightarrow \bar{D}^0 f_2^q) = \frac{G_F}{\sqrt{2}} \frac{1}{\sqrt{2}} V_{cb}^* V_{ud} [a_2 \mathcal{A}_{af} + C_2 \mathcal{M}_{anf} + a_2 \mathcal{A}_{ef} + C_2 \mathcal{M}_{enf}], \quad (B17)$$

$$\mathcal{A}(B^0 \rightarrow \bar{D}^0 K_2^{*0}) = \frac{G_F}{\sqrt{2}} V_{cb}^* V_{us} [a_2 \mathcal{A}_{ef} + C_2 \mathcal{M}_{enf}], \quad (B18)$$

$$\mathcal{A}(B^0 \rightarrow D^- a_2^+) = \frac{G_F}{\sqrt{2}} V_{cb}^* V_{ud} [C_1 \mathcal{M}_{enf}^3 + a_2 \mathcal{A}_{af} + C_2 \mathcal{M}_{anf}], \quad (B19)$$

$$\mathcal{A}(B^0 \rightarrow D^- K_2^{*+}) = \frac{G_F}{\sqrt{2}} V_{cb}^* V_{us} [C_1 \mathcal{M}_{enf}^3], \quad (B20)$$

$$\mathcal{A}(B^0 \rightarrow D_s^- K_2^{*+}) = \frac{G_F}{\sqrt{2}} V_{cb}^* V_{ud} [a_2 \mathcal{A}_{af} + C_2 \mathcal{M}_{anf}], \quad (B21)$$

$$\mathcal{A}(B^+ \rightarrow \bar{D}^0 a_2^+) = \frac{G_F}{\sqrt{2}} V_{cb}^* V_{ud} [a_2 \mathcal{A}_{ef} + C_2 \mathcal{M}_{enf} + C_1 \mathcal{M}_{enf}^3], \quad (B22)$$

$$\mathcal{A}(B^+ \rightarrow \bar{D}^0 K_2^{*+}) = \frac{G_F}{\sqrt{2}} V_{cb}^* V_{us} [a_2 \mathcal{A}_{ef} + C_2 \mathcal{M}_{enf} + C_1 \mathcal{M}_{enf}^3], \quad (B23)$$

$$\mathcal{A}(B_s^0 \rightarrow \bar{D}^0 f_2^q) = \frac{G_F}{\sqrt{2}} \frac{1}{\sqrt{2}} V_{cb}^* V_{us} [a_2 \mathcal{A}_{af} + C_2 \mathcal{M}_{anf}], \quad (B24)$$

$$\mathcal{A}(B_s^0 \rightarrow \bar{D}^0 a_2^0) = \frac{G_F}{\sqrt{2}} \frac{1}{\sqrt{2}} V_{cb}^* V_{us} [a_2 \mathcal{A}_{af} + C_2 \mathcal{M}_{anf}], \quad (B25)$$

$$\mathcal{A}(B_s^0 \rightarrow \bar{D}^0 f_2^s) = \frac{G_F}{\sqrt{2}} V_{cb}^* V_{us} [a_2 \mathcal{A}_{ef} + C_2 \mathcal{M}_{enf}], \quad (\text{B26})$$

$$\mathcal{A}(B_s^0 \rightarrow \bar{D}^0 \bar{K}_2^{*0}) = \frac{G_F}{\sqrt{2}} V_{cb}^* V_{ud} [a_2 \mathcal{A}_{ef} + C_2 \mathcal{M}_{enf}], \quad (\text{B27})$$

$$\mathcal{A}(B_s^0 \rightarrow D^- a_2^+) = \frac{G_F}{\sqrt{2}} V_{cb}^* V_{us} [a_2 \mathcal{A}_{af} + C_2 \mathcal{M}_{anf}], \quad (\text{B28})$$

$$\mathcal{A}(B_s^0 \rightarrow D_s^- a_2^+) = \frac{G_F}{\sqrt{2}} V_{cb}^* V_{ud} [C_1 \mathcal{M}_{enf}^3], \quad (\text{B29})$$

$$\mathcal{A}(B_s^0 \rightarrow D_s^- K_2^{*+}) = \frac{G_F}{\sqrt{2}} V_{cb}^* V_{us} [a_2 \mathcal{A}_{af} + C_2 \mathcal{M}_{anf} + C_1 \mathcal{M}_{enf}^3]. \quad (\text{B30})$$

- [1] K. Nakamura et al. [Particle Data Group], J Phys. G **37**, 075021 (2010).
- [2] Wei Wang, Phys. Rev. D **83**, 014008 (2011).
- [3] C. S. Kim, B. H. Lim and S. Oh, Eur. Phys. J. C **22**, 683 (2002) [arXiv:hep-ph/0101292].
- [4] C. S. Kim, B. H. Lim and S. Oh, Eur. Phys. J. C **22**, 695 (2002) [Erratum-ibid. C **24**, 665 (2002)] [arXiv:hep-ph/01080504].
- [5] C. S. Kim, B. H. Lim and S. Oh, Phys. Rev. D **67**, 014002 (2003) [arXiv:hep-ph/0205263].
- [6] J. H. Muñoz and N. Quintero, J. Phys. G **36**, 095004 (2009) [arXiv:0903.3701 [hep-ph]].
- [7] N. Sharma and R. C. Verma, arXiv:1004.1928 [hep-ph].
- [8] H. Y. Cheng, Y. Koike and K. C. Yang, Phys. Rev. D **82**, 054019 (2010) [arXiv:1007.3541 [hep-ph]].
- [9] Hai-Yang Cheng and Kwei-Chou Yang, Phys. Rev. D **83**, 034001 (2011) [arXiv:1010.3309 [hep-ph]].
- [10] Z. T. Zou, X. Yu and C. D. Lü, arXiv:1203.4120 [hep-ph].
- [11] A. C. Katoch and R. C. Verma, Phys. Rev. D **49**, 1645 (1994); **52**, 1717 (1995); **55**, 7315(E) (1997).
- [12] G. López Castro and J. H. Muñoz, Phys. Rev. D **55**, 5581 (1997) [arXiv:hep-ph/9702238].
- [13] J. H. Muñoz, A. A. Rojas, and G. López Castro, Phys. Rev. D **59**, 077504 (1999).
- [14] N. Sharma, R. Dhir and R. C. Verma, Phys. Rev. D **83**, 014007 (2011) [arXiv:1010.3077 [hep-ph]].
- [15] C. S. Kim, B. H. Lim and S. Oh, Phys. Rev. D **67**, 014011 (2003).
- [16] Wei Wang, Phys. Rev. D **85**, 051301 (2012).

- [17] Z. T. Zou, Zhou Rui and C. D. Lü, arXiv:1204.3144 [hep-ph].
- [18] Y. Y. Keum, H. n. Li and A. I. Sanda, Phys. Lett. B **504**, 6 (2001) [arXiv:hep-ph/0004004]; Phys. Rev. D **63**, 054008 (2001) [arXiv:hep-ph/0004173].
- [19] C. D. Lü, K. Ukai and M. Z. Yang, Phys. Rev. D **63**, 074009 (2001) [arXiv:hep-ph/0004213].
- [20] C. D. Lü, K. ukai, Eur. Phys. J. C **28**, 305 (2003) [arXiv:hep-ph/0210206].
- [21] Y. Li, C. D. Lü, J. Phys. G **29**, 2115 (2003) [arXiv:hep-ph/0304288]; High Energy Phys. & Nucl. Phys. **27**, 1062 (2003) [arXiv:hep-ph/0305278].
- [22] H. n. Li, Phys. Rev. D **52**, 3958 (1995) [arXiv:hep-ph/9412340]; C. Y. Wu, T. W. Yeh and H. n. Li, Phys. Rev. D **53**, 4982 (1996) [arXiv:hep-ph/9510313]; Y. Y. Keum et al., Phys. Rev. D **69**, 094018 (2004); C. D. Lü, Phys. Rev. D **68**, 097502 (2003).
- [23] C. D. Lü, Eur. Phys. J. C **24**, 121-126 (2002); J. F. Cheng, D. S. Du and C. D. Lü, Eur. Phys. J. C **45**, 711 (2006).
- [24] C. W. Bauer, D. Pirjol, I. Z. Rothstein and I. W. Stewart, Phys. Rev. D **70**, 054015 (2004).
- [25] G. Buchalla, A. J. Buras and M. E. Lautenbacher, **Rev. Mod. Phys.** **68** (1996) 1125; A.J. Buras, [hep-ph/9806471].
- [26] H. N. Li, Phys. Rev. D **66**, 094010 (2002)
- [27] H. N. Li and B. Tseng, Phys. Rev. D **57**, 443 (1998)
- [28] C. D. Lü and M. Z. Yang, Eur. Phys. J. C **23**, 275-287 (2002).
- [29] C. D. Lü and M. Z. Yang, Eur. Phys. J. C **28**, 515 (2003).
- [30] T. Kurimoto, H. n. Li and A. I. Sanda, Phys. Rev. D **65**, 014007 (2002).
- [31] Z. T. Wei and M. Z. Yang; Nucl. Phys. B **642**, 263 (2002).
- [32] A. Ali, et al., Phys. Rev. D **76**, 074018 (2007).
- [33] T. Kurimoto, H. n. Li and A. I. Sanda, Phys. Rev. D **67** 054028 (2003).
- [34] R. H. Li, C. D. Lü and H. Zou, Phys. Rev. D **78** 014018 (2008).
- [35] H. Zou, R. H. Li, X. X. Wang and C. D. Lü, J. Phys. G **37**, 015002 (2010).
- [36] R. H. Li, C. D. Lü, A. I. Sanda, X. X. Wang, Phys. Rev. D **81**, 034006 (2010).
- [37] E. Follana, C. T. H. Davies, G. P. Lepage and J. Shigemitsu [HPQCD Collaboration and UKQCD Collaboration], Phys. Rev. Lett. **100**, 062002 (2008).
- [38] A. V. Manohar and M. B. Wise, Camb. Monogr. Part. Phys. Nucl. Phys. Cosmol. 10, 1 (2000).
- [39] J. G. Körner and G. R. Goldstein, Phys. Lett. **B79**, 105 (1979).

- [40] A. L. Kagan, Phys. Lett. **B601**, 151 (2004).
- [41] A. V. Gritsan, eConf. C **070512**,001 (2007).
- [42] T. M. Aliev and M. A. Shifman, Phys. Lett. B **112**, 401 (1982); Sov. J. Nucl. Phys. **36**, 981 (1982) [Yad. Fiz. **36**, 1532 (1982)].
- [43] T. M. Aliev, K. Azizi and V. Bashiry, J. Phys. G **37**, 025001 (2010). **48**, 339 (1993).
- [44] Hai-Yang Cheng and Robert Shrock, Phys. Rev. D **84**, 094008 (2011) [arXiv:hep-ph/1109.3877].
- [45] D. M. Li, H. Yu, and Q. X. Shen, J. Phys. G **27**, 807 (2001).
- [46] H.-n. Li and K. Ukai, Phys. Lett. B **555**, 197 (2003).